

AMERICAN UNIVERSITY OF BEIRUT

RELIABILITY BASED ANALYSIS OF SPATIALLY RANDOM
COHESIVE MULTI-LAYERED SLOPES

by
REEM ATEF JABER

A thesis
submitted in partial fulfillment of the requirements
for the degree of Master of Engineering
to the Department of Civil and Environmental Engineering
of the Maroun Semaan Faculty of Engineering and Architecture
at the American University of Beirut

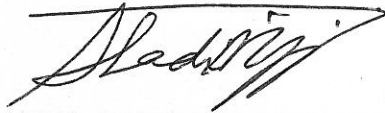
Beirut, Lebanon
April 17th, 2018

AMERICAN UNIVERSITY OF BEIRUT

RELIABILITY BASED ANALYSIS OF SPATIALLY RANDOM
COHESIVE MULTI-LAYERED SLOPES

by
REEM ATEF JABER

Approved by:



Dr. Shadi Najjar, Associate Professor
Civil and Environmental Engineering

Advisor



Dr. Salah Sadek, Professor
Civil and Environmental Engineering

Co-Advisor



Dr. Ibrahim Alameddine, Assistant Professor
Civil and Environmental Engineering

Member of Committee

Date of thesis defense: April 17th, 2018

AMERICAN UNIVERSITY OF BEIRUT

THESIS, DISSERTATION, PROJECT RELEASE FORM

Student Name: JABER REEM ATEF
Last First Middle

Master's Thesis Master's Project Doctoral Dissertation

I authorize the American University of Beirut to: (a) reproduce hard or electronic copies of my thesis, dissertation, or project; (b) include such copies in the archives and digital repositories of the University; and (c) make freely available such copies to third parties for research or educational purposes.

I authorize the American University of Beirut, to: (a) reproduce hard or electronic copies of it; (b) include such copies in the archives and digital repositories of the University; and (c) make freely available such copies to third parties for research or educational purposes
after: One year from the date of submission of my thesis, dissertation, or project.
Two X years from the date of submission of my thesis, dissertation, or project.
Three years from the date of submission of my thesis, dissertation, or project.

Handwritten signature of Jaber

Handwritten date: 14/05/2018

Signature

Date

ACKNOWLEDGMENTS

As this project wraps, I extend my deepest gratitude to the people without whom it would not have been possible: first and foremost my advisers and mentors: professors Shadi Najjar and Salah Sadek. Your encouragement, guidance, and patience have made all the difference and propelled this project forward through all the seemingly-dead ends. Your guidance kept me on track, and for that I thank you.

Further, I thank Mr. Ahmad Kahiel for his enormous help and support in R software. I also thank my parents for being the best support system a student could ask for and for helping me through the difficult times that come with writing theses.

AN ABSTRACT OF THE THESIS OF

Reem Atef Jaber for Master of Engineering
Major: Geotechnical Engineering

Title: Reliability Based Analysis of Spatially Random Cohesive Multi-layered Slopes

Slope stability is a branch of geotechnical engineering that is affected significantly by uncertainty due to spatial variability of soil properties. Traditional deterministic slope stability design methodologies account for these uncertainties in an indirect manner by adopting a target factor of safety that is generally equal to 1.5. In the last two decades, results from published reliability-based design methods for slopes indicated that even for the case of a simple homogeneous slope, a factor of safety of 1.5 may not lead to designs that have a consistent level of risk. More importantly, published results show lack of knowledge about the reliability levels that are inherent in the design of multi-layered slopes which are very common in applications involving compacted embankments over soft clays or in natural multi-layered slopes. The main objectives of this thesis are twofold. The first objective is to quantify the reliability levels that are inherent in spatially random multi-layered clayey slopes with different thicknesses and soil properties. The second objective is to generate simplified equations that would allow for conducting reliability-based design for a two-layered slope system using only the deterministic results and the input soil properties. To achieve these objectives, Monte Carlo simulations that involve clayey slopes with multiple layers are performed using the finite difference software FLAC. To allow for realistic modeling of the failure surface in the multi-layered system, FISH functions were used in FLAC to model the spatial variability using realistic anisotropic random fields that would ensure a realistic representation of the soil properties in the multi-layered slope and result in probabilities of failure that reflect the real level of risk. The models generated to predict the behavior when accounting for spatial variability in soil will lead to improved design practices for multi-layered clayey slopes.

CONTENTS

ACKNOWLEDGEMENTS	v
ABSTRACT.....	vi
LIST OF ILLUSTRATIONS.....	xi
LIST OF TABLES.....	xv

Chapter

I. INTRODUCTION.....	1
A. Background	1
B. Objectives and Scope of Research.....	4
II. LITERATURE REVIEW	6
A. Studies Involving LEM with Random Field Theory	6
B. Studies Involving the Random Finite Element Method	9
C. Studies of Multi-Layered Slope Systems.....	12
III. FLAC SOFTWARE.....	21
A. Background.....	21
B. Input Parameters.....	22

1. Slope Generation	22
2. Finite Difference Grid/Mesh.....	22
3. Finite Difference Zone/Element.....	23
4. Boundary Conditions.....	24
5. Number of Realizations.....	24
6. Constitutive Model.....	25
7. Strength Reductions.....	25
8. Spatial Correlation.....	26
9. Friction Angle.....	31
10. Elastic Modulus.....	31
11. Poisson's Ratio.....	31
12. Mass Density.....	31
C. Probabilistic Distribution of Shear Strength.....	31
1. Lognormal Distribution.....	31
2. Local Averaging.....	33
3. Generating and Mapping of Random Fields	34
IV. DETERMINISTIC ANALYSIS OF MULTI-LAYERED CLAYEY SLOPES.....	39
A. Slope Parameters.....	39
B. FLAC Stability Results.....	40
C. Effect of the Undrained Shear Strength of the top layer (c_{u1}).....	44
D. Regression Model for the Deterministic Dimensionless Stability Number (N).....	46
V. STABILITY RESULTS FOR SPATIALLY VARIABLE TWO-LAYERED CLAYEY SLOPES.....	48
A. Introduction.....	48
B. Effect of Random Field of c_{u1} and c_{u2} on Mode of Failure.....	49
C. Analysis of Spatially Random Two-layered Slopes.....	51
1. Effect of c_{u1}/c_{u2} , d/H , and COV c_u on Probabilistic Stability	52
2. Effect of the Scale of Fluctuation (SOF) on Statistics of N.....	58
3. Effect of the Slope Inclination Angle (β) on Statistics of N.....	61

VI. RELATIONSHIP BETWEEN DETERMINISTIC AND PROBABILISTIC RESULTS.....	64
A. Relationship between N_m/N_d and COV c_u	64
B. Relationship between N_m/N_d and c_{u1}/c_{u2}	66
C. Relationship between COV N /COV c_u and c_{u1}/c_{u2}	67
D. Relationship between COV N /COV c_u and $\delta y/LFS$	69
VII. RELIABILITY DESIGN OF SPATIALLY VARIABLE MULTI-LAYERED CLAYEY SLOPES.....	71
A. Mean of N as a function of COV c_u	71
B. (COV N /COV c_u) as a function of (δy /length of failure surface) in Multi-Layered Slopes.....	73
C. Regression Models for Predicting Mean and COV of N	74
1. Regression Model for (N_m/N_d)	74
2. Regression Model for (COV N /COV c_u).....	76
VII. DESIGN EXAMPLE.....	78
IX. CONCLUSIONS.....	82
<i>Appendix</i>	
I. FLAC CODE.....	86
II. R SOFTWARE CODE.....	92
II. R SOFTWARE CODE.....	96

BIBLIOGRAPHY..... 97

ILLUSTRATIONS

Figure	Page
1. Stability of the embankment over stone columns considering water table (Abusharar and Han 2011).	13
2. Profile of a slope and typical realization of random fields with slope stability results (Li et al., 2014).....	14
3. Chart Results for slope angle of 60° (Qian et al., 2015)	15
4. Geometry of Slope Considered in Hong et al. (2016)	16
5. Example of factor of Safety Results (Hong et al., 2016)	16
6. Results obtained from three-layered cohesive slope for no ISV and ISV respectively (Li et al., 2016).....	17
7. Realization of random field with ISV (Li et al., 2016)	17
8. Random Field Realization for Soil properties (Liu et al., 2017).....	19
9. Effect of COV and SOF on probability of failure (Liu et al., 2017).....	19
10. Effect of Correlation Length on risk of slope failure for the proposed approach and the limit analysis-based MCS (Jiang et al., 2017).....	20
11. Medium Mesh Slope Geometry.....	23
12. Realization with isotropic random field $\delta=40\text{m}$	29
13. Realization with isotropic random field $\delta=2\text{m}$	30
14. Realization with (a) isotropic random field $\delta_x = \delta_y = 2\text{m}$ and (b) anisotropic random field with $\delta_x = 40\text{m}$ and $\delta_y = 2\text{m}$	30
15. Slope geometry in FLAC.....	39

16.	Variation of N_d with respect to d/H , c_{u1}/c_{u2} , and β	42
17.	Shadings of the Maximum Shear Strain Increment for samples of the two-layered slope cases analyzed (Shear strain increment increases from red, to orange, to yellow, to green and finally to blue.....)	43
18.	Performance of Regression Model based on 20 Independent Analysis Cases.....	47
19.	Slope geomtery with main input parameters.....	49
20.	Different failure surfaces for random realizations.....	50
21.	The mean factor of safety with respect to c_{u1}/c_{u2} for different d/H	51
22.	F.S _m with respect to c_{u1}/c_{u2} for different d/H for COV $c_u = 0.5$ & 0.3	53
23.	COV of F.S with respect to c_{u1}/c_{u2} for different d/H and for COV $c_u = 0.5$ & 0.3	53
24.	N_m with respect to c_{u1}/c_{u2} for different d/H and for COV $c_u = 0.5$ and 0.3	56
25.	COV of N with respect to c_{u1}/c_{u2} for different d/H and for COV $c_u = 0.5$ and 0.3	56
26.	Comparison between the pdf and cdf of N distribution and a lognormal distribution.....	58
27.	QQ-plot between N distribution and lognormal distribution.....	58
28.	N_m vs. c_{u1}/c_{u2} for COV $c_u = 0.5$ & 0.3	59
29.	Comparison between COV of N for $\delta y = 1, 2$ & $5m$ for COV $c_u = 0.5$ & 0.3	60

30.	Comparison between COV of N for $\delta_y=1, 2\&5m$ for COV $c_u=0.5$	61
31.	Comparison between N_m for $\beta=30^\circ, 45^\circ,$ and 60° for COV $c_u=0.5$	62
32.	Comparison between COV of N for $\beta=30^\circ, 45^\circ,$ and 60°	62
33.	N_m/N_d with respect to COV c_u for $\beta=30^\circ, \beta=45^\circ,$ and $\beta=60^\circ$	65
34.	N_m/N_d with respect to c_{u1}/c_{u2} for $\beta=30^\circ$	66
35.	Dependence of COV N_m /COV c_u on Input Parameters ($\beta = 30^\circ$).....	68
36.	COV N /COV c_u with respect to $\delta_y/L.FS$	70
37.	Model for N_m/N_d vs. COV c_u	72
38.	Effectiveness of Model Predictions of Equation 7.1.....	72
39.	COV N /COV c_u with respect to $\delta_y /L. FS$ for COV $c_u=0.5\&0$	73
40.	Effectiveness of Equation 7.2 in predicting the ratio of COV N /COV c_u	74
41.	Effectiveness of Equation 7.4 in predicting the ratio of N_m/N_d	76
42.	Effectiveness of Equation 7.5 in predicting the ratio of COV N /COV c_u	77
43.	Geometry and Soil Properties of the illustrative Design Example.....	78

44.	Probability of failure (pf) vs. FS design.....	81
45.	Embankment Height (H) vs. COV c_u	81

TABLES

Table		Page
1.	Sensitivity of the Results of N_d and N_m to the choice of c_{u1}	45
2.	The values of the main factors in the N_m and COV N equations for the validation cases.....	96

CHAPTER I

INTRODUCTION

A. Background

Slope stability is a branch of geotechnical engineering that is affected by uncertainty due to spatial variability of soil properties. Traditional design approaches for slopes adopt a target global factor of safety (FS) of 1.5 to account for these uncertainties (Terzaghi and Peck, 1948). The deterministic analysis methods use the Limit Equilibrium (LEM) or Finite Element Method (FEM) to calculate the factor of safety. Given the different sources of uncertainty affecting slope stability problems, designs that are based on a fixed factor of safety of 1.5 may not lead to reliable designs. A probabilistic design approach can incorporate all sources of uncertainty and lead to quantification of the probability of failure of the slope and its level of risk (Griffiths et al. 2009).

Previous published work has shown that the use of a single factor of safety cannot result in a consistent measure of reliability. Results of Li and Lumb (1987) showed that slopes that are designed with the same FS may have different levels of risk depending on the variability of the soil properties. Although soil properties are rarely homogeneous by nature and vary spatially due to different depositional environments and loading histories, most slope stability methods ignore the spatial variation of soil properties (Hong et al., 2008). In the late 90's, and as a result of limitations that are associated with the Limit Equilibrium Method (LEM) in relation to the relatively rigid choice of the shape and location of the failure surface, slope stability analyses that are based on the finite element

method started grasping more attention. Griffiths and Lane (1999) were the first to present the finite element method in analyzing slope stability problems which relaxed the choice of the failure surface with regards to shape and location.

The finite element method was later combined with random field theory to produce the Random Finite Element Method (RFEM) after it was shown to have a clear advantage over the LEM, given its ability to model the spatial variation of soil properties to resemble natural deposition of soil layers. The RFEM was used to investigate the effect of spatial variability of soil parameters on the failure probabilities of single-layered slopes with different heights, angles, and soil properties. The RFEM was first applied by Fenton and Griffiths (2000) who established a dedicated Software for this purpose.

For cases involving clayey slopes, results from RFEM analyses indicated that the most important parameters affecting the probability of failure of spatially random slopes are: (1) the assumed factor of safety, (2) the degree of uncertainty in the undrained shear strength of the clay, and (3) the vertical and horizontal scales of fluctuation that define the degree of correlation which exists in the random field defining the uncertainty in the undrained shear strength, and (4) the height of the slope which is directly correlated with the length of the failure surface around which the soil properties vary. Jha and Ching (2013) present relationships which link the mean factor of safety and the coefficient of variation in the factor of safety of an undrained slope to the deterministic factor of safety, the COV of the undrained shear strength, the ratio of the vertical scale of fluctuation to the length of the failure surface, and the ratio of the horizontal scale of fluctuation to the vertical scale of fluctuation. These relationships were obtained from results of random finite element

analyses and allow for estimating the probability of failure of any single-layered spatially variable clayey slope.

The proposed research aims at extending the use of the RFEM to cases involving multi-layered slopes. Slopes that consist of several soil layers are more complex to analyze given the contrast in the soil properties between the multiple layers. Results from deterministic studies on multi-layered slopes point to this complexity. There is a need for modeling the spatial variability in the soil properties within the multi layers using random field theory to enhance the understanding of the reliability of multi-layered slopes in cohesive soils.

This thesis is divided as follows: Chapter II is a literature review narrating the evolution of slope stability analysis methods throughout the years. Chapter III includes a background about the software FLAC used. Chapter IV states the deterministic results of FLAC while Chapter V shows the results accounting for the spatial variability of soil properties. Chapter VI discusses the relationship between probabilistic and deterministic results as a function of the main factors that may affect the problem and Chapter VII presents models to simplify reliability based design for two-layered cohesive slopes. Finally, a design example is shown in Chapter VIII and Chapter IX summarizes the main findings of this research.

B. Objectives and Scope of Research

In clayey slopes, the uncertainty is mostly associated with the undrained shear strength of the clay, which governs the probability of failure. Most of the aforementioned studies focused on homogeneous slope cases that could be modeled using a single-layer system, except for Abusharar and Han (2011) , Li et al. (2014), Qian et al. (2015), Hong et al. (2016), Li et al. (2016), Liu et al. (2017) and Jiang et al. (2017) who analyzed two- and three-layered systems. In the papers dealing with multi-layered systems, the focus was on new analysis methods or new probabilistic approaches rather than systematically studying the factors that affect the factor of safety and probability of failure of the multi-layered system.

The main objective of this thesis is to study the effect of spatial variability on the probability of failure of two-layered slopes with clay layers of contrasting undrained strength. The focus will be on practical scenarios that involve a stiff clay layer on top of a soft clay layer. Examples of these cases include but are not limited to compacted clay embankments laying on a natural clay and natural cut slopes that are composed of multiple layers with different nature or consistency. The reliability of spatially random cohesive multi-layered slopes will be assessed for a wide variety of slope geometries and soil conditions and for different soil correlation structures.

The proposed scope of work is composed of several steps for achieving the objectives.

1. Conduct a comprehensive literature review on methods of slope stability analysis for spatially variable single and multi-layered clayey slopes.
2. Establish a methodology for conducting Monte Carlo Simulations for multi-layered spatially random slopes using FLAC 2D.
3. Analyze the impact of the major input parameters on the uncertainty in the resulting factor of safety (FS) and the stability number (N).
4. Design and implement a parametric study for quantifying the reliability of two-layered undrained clayey slope.

CHAPTER II

LITERATURE REVIEW

This section depicts a literature review showing some of the previous work done on the role of spatial variability in slope stability analysis following limit equilibrium methods (LEM) in addition to subsequent finite element methods (FEM) using several software programs. The quest to incorporate uncertainty in soil properties in the design of slopes was initiated by Venmarcke (1977) who shed light for the first time on the significance of spatial correlation between soil properties and its effect on the probability of failure of slopes. This was followed by work published by Li and Lumb (1987), Malkawi et al. (2000), Cho (2007 and 2010), and Wang et al. (2011), who investigated spatial variability in slope stability using limit equilibrium methods.

A. Studies Involving LEM with Random Field Theory

Li and Lumb (1987) were among the early pioneers of utilizing a probabilistic approach in slope stability analysis using LEM with random field theory. The method used in performing LEM was the Morgenstern and Price Method. The authors used the First Order Second Moment (FOSM) method in calculating the reliability of slopes. Li and Lumb assumed an isotropic correlation in soil properties between elements. This assumption yielded an overestimation in failure probabilities. The results showed the sensitivity of the probability of failure to the scale of fluctuation, thus recommending better estimation of the scale of fluctuation. They concluded that the deterministic critical slip surface can serve as a good initial guess in the reliability analysis.

Low (2003) applied a procedure to implement Spencer's method of slices in deterministic and probabilistic approaches using a spreadsheet-automated optimization to calculate the reliability index. The deterministic approach was then extended to the probabilistic approach with constrained dispersion of the original space of random variables. The results of the probabilities of failure and probability density functions computed indicated good and acceptable values with respect to the ones computed by the Monte Carlo Simulation method.

Babu and Mukesh (2004) also modeled spatial variation in slope stability problems. They assumed a simple cohesive soil with definite geometry and soil properties. The authors took two cases into consideration, assuming isotropic and anisotropic correlations in soils properties. Their results showed that the mean factor of safety, as well as the coefficient of variation and correlation distance, can affect the calculated probability of failure. Also, the study concluded that assuming isotropic correlation distance results in an overestimated probability of failure, which raises the need to account for anisotropic correlation in slope stability analysis.

Cho (2007) presented a numerical procedure for probabilistic slope stability analysis using Monte Carlo simulations while accounting for spatial variations in slope properties. The stability analyses were done on layered slopes to study the effect of uncertainty. The results showed some differences in the locations of the probabilistic and deterministic critical failure slope. Cho concluded that the correlation characteristics of soil properties significantly affect the probabilities of failure and convergence of the analysis and found the assumption of isotropic field to be conservative. Cho also deduced that there

exists a relation between the probability of failure and the scale of fluctuation. The probability of failure was found to decrease as the scale of fluctuation decreased. The results point to the importance of incorporating spatially variability of soil properties in soil stability analysis.

Cho (2010) used the Karhunen-Loeve Expansion method in generating random fields and used Monte Carlo simulations to calculate the statistics of the factor of safety. The strength reduction method was used in calculating the factor of safety and adapted a search concept based on finding the surface with the minimum reliability index. No previous assumptions were made about the critical failure surface. The stability analysis, based on strength reduction method, was conducted using FLAC (How is this an LEM method?). Cho concluded in his paper that the proposed method considers various failure mechanisms efficiently.

Wang et al. (2011) studied slope stability analysis using a probabilistic approach that is based on “subset simulation”, an advanced MCS method that could improve the efficiency and resolution of MCS at low failure probabilities. The analysis is implemented using a spreadsheet package in Microsoft Excel to investigate the effect of spatial variability. Wang et al. found that ignoring spatial variability by assuming perfect correlation results in overestimating the variance of the factor of safety, especially if the effective correlation length is smaller than the slope height. Wang et al. recommended the spatial variability of soil properties to be accounted for accurately to prevent errors in the probability of failure.

B. Studies Involving the Random Finite Element Methods

All the studies presented above used the limit equilibrium method with the random field theory. This approach limits the influence of the random field to the failure line only, rendering the randomness one-dimensional. Therefore, the need for a new method that can overcome the limitation proposed by LEM became evident, and the random finite element method (RFEM) was established to serve this purpose. RFEM combines nonlinear finite element methods with random field generation. This approach soon became a powerful tool in slope stability analysis, fully capturing the soil spatial correlation and averaging. It also does not require any priori assumptions of the failure mechanism regarding shape or location. The pioneers of this approach were Griffiths and Fenton, followed by many researchers who focused on this method in slope stability analysis.

Griffiths and Fenton (2000) conducted a probabilistic study on undrained clay slopes focusing on the effect of the scale of fluctuation and the coefficient of variation of soil properties. The results showed that as the coefficient of variation increases, the probability of failure increases. This study deduced that assuming perfect correlation resulted in over estimation in the probability of failure in case of low COV and high factor of safety ($FS > 1.4$) and underestimation in the probability of failure in opposite cases. Griffiths and Fenton (2004) compared simple and probabilistic approaches for a cohesive undrained slope. The results using RFEM showed that combining both concepts of spatial correlation with local averaging yielded smaller probabilities of failure. Griffiths and Fenton reassured that RFEM overcomes LEM limitations by the absence of any assumptions of the failure surface.

Griffiths et al. (2009) investigated the probability of failure of both 2D and 3D slopes using RFEM for deterministic and probabilistic analyses. The results showed that 2D analysis results were non-conservative to a certain limit and were affected by the boundary conditions of the out of plane direction and length to height ratios. Griffiths et al. (2010) made a comparison among different methods of the limit equilibrium method: Point Estimate Method, First Order Second Moment Method, and First Order Reliability Method with the random finite element method in slope analysis problem. It was concluded that RFEM is superior to LEM.

The random finite element analysis was later extended to applications involving random finite difference analyses. The finite difference software FLAC was generally used in these studies as the main calculation platform. Srivastava (2012) conducted random finite difference analyses of slope stability using FLAC. Soil parameters were modeled using lognormally-distributed 2D random fields with their spatial correlation properties modeled using Cholesky decomposition. The study re-confirmed the finding that incorporating spatial variation using random fields is required to ensure realistic factors of safety compared with conventional limit equilibrium-based factor of safety. Results indicated that by increasing the coefficient of variation, there is a decrease in the reliability index. On the other hand, increasing the correlation distance results in a decrease in the reliability index.

Jha and Ching (2013) studied the effect of slope geometry, mean, and coefficient of variation of the soil properties and the scale of fluctuation on the probabilities of failure of undrained slopes using RFEM. The scale of fluctuation in the vertical direction was back

calculated from a database of 34 real undrained slope cases. The horizontal scale of fluctuation was assumed due to the lack of data. An added value of this paper was providing relationships between the mean and coefficient of variation of the factor of safety, and between the mean and coefficient of variation of soil parameters and the slope geometry. The authors showed that the mean FS and its COV are always less than the deterministic FS and the COV describing the uncertainty in the undrained shear strength, respectively. In both cases, the reduction is most shown when the inherent COV is large.

Li et al. (2015) integrated RFEM with advanced Monte Carlo Simulation (MCS) method called “Subset Simulation (SS)” to eliminate the exhaustive computational efforts, especially at small probabilities in reliability analysis of soil slopes. The results obtained from the SS-based RFEM were validated against those obtained using the direct MCS based RFEM. Results of the paper demonstrated the improved computational time for computing probability of failure and risk of the slope. In addition, the sensitivity study presented the significant effect of vertical spatial variability on the slope failure risk. Furthermore, Li et al. (2016) combined LEM with FEM in a new probabilistic approach to get advantage of fast computational time with more realistic results. The results showed significant reduction in the time and in the number of finite element analyses time at low probabilities of failure.

On the other hand, Jiang et al. (2016) presented a new approach based on multiple response surface method and Subset simulation and using improved Cholesky decomposition techniques for calculating small probabilities of failure of spatially variable soil for multiple soil layered system. The paper concluded that the proposed methodology

can estimate small probabilities of failure with high computational efficiency for circular slip surfaces. However more research is required to investigate non-circular slip surfaces.

In the most recent study, Griffiths et al. (2017) used the random finite element method to investigate spatial variability effects based on non-stationary random fields in undrained slopes. They assumed that the mean undrained shear strength varied linearly with depth with a COV that is depth independent. The results were divided based on low or high levels of COV and were found to be sensitive to what the authors call the “seeking out” phenomenon in which deeper failure mechanisms can be attracted to low strengths at greater depths generated by the random field.

C. Studies of Multi-layered Slope Systems

Abusharar and Han (2011) used the finite difference Software FLAC for estimating the factor of safety in embankments over stone-column-improved soft clay (Fig. 1) based on individual and equivalent area models. The paper investigated the factors influencing the factor of safety including the properties of the embankment fill, cohesion of soft clay, friction angle of stone columns, and ground water. Results indicated higher factors of safety using equivalent area models in comparison to individual area models. Lower factors of safety were also observed when ground water is incorporated in the model since pore pressure reduced the frictional shear strength.

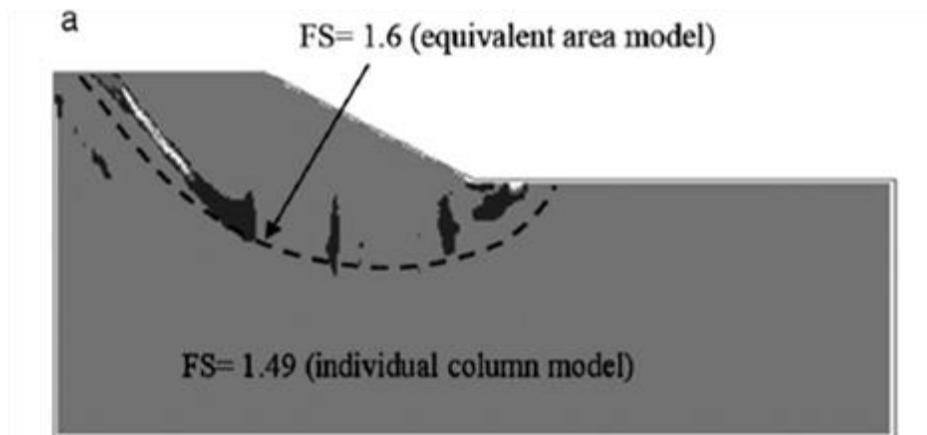


Figure 1. Stability of the embankment over stone columns considering water table (Abusharar and Han 2011)

Li et al. (2014) proposed a multiple response-surface method for slope stability analysis accounting for spatial variability of soil parameters using extended Cholesky decomposition. The authors studied the effect of five different theoretical autocorrelation functions to model the spatial variability. A three-layered slope case was used to validate the effectiveness of the proposed method as shown in Figure 2. The results proved the proposed method suggested by the authors to be a practical tool for assessing slope stability analysis for spatially variable soils. The computational efficiency was enhanced especially for relatively low-probability analysis. The paper concluded that the difference between the probabilities of failure corresponding to each autocorrelation function is minimal.

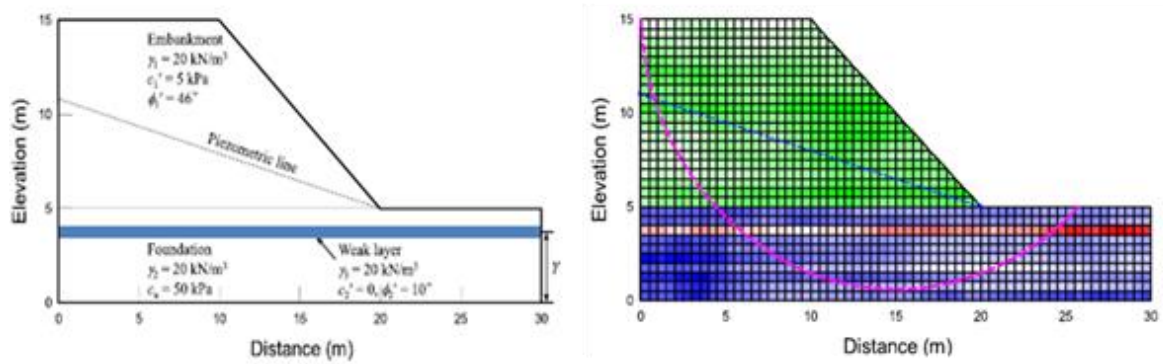


Figure 2. Profile of a slope and typical realization of random fields with slope stability results (Li et al., 2014)

Qian et al. (2015) proposed stability charts for cohesive soil slopes as a design tools. These charts were produced using finite element upper and lower bound limit analysis and compared with LEM methods. The slope material and subgrade foundation material of the slope were of two different undrained shear strengths. Results were presented and compared in the form of a dimensionless stability number (N_{2c}) for a range of slope inclinations, depth factors, and strengths ratios. Differences in (N_{2c}) between numerical limit methods and LEM methods reached 20%. It was concluded that the predetermined circular slip surface in LEM is not always suitable for evaluating two-layered slopes. Fig. 3 is an example of chart results presented for a slope angle of 60 degrees.

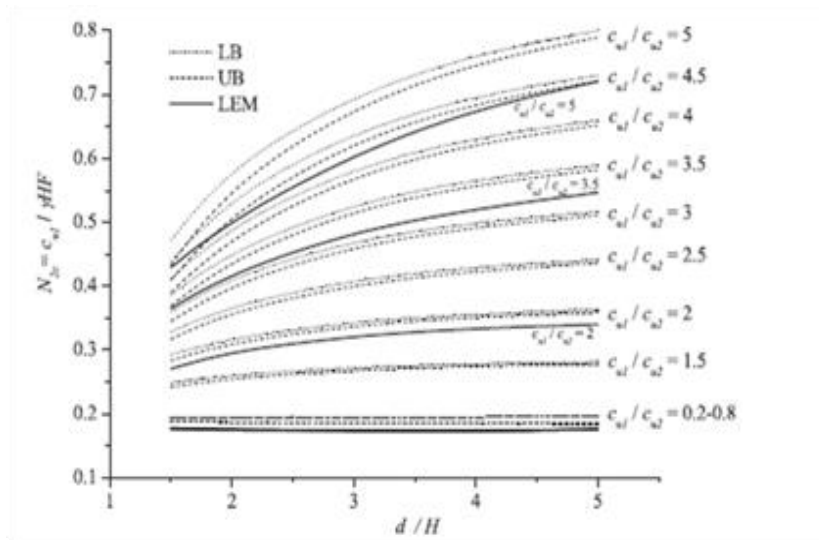


Figure 3. Chart Results for slope angle of 60° (Qian et al., 2015)

Hong et al. (2016) proposed a practical method that combines finite difference method with random field theory for probabilistic slope stability analysis based on Monte Carlo simulations. The factor of safety was estimated using the strength reduction method and a two-layer slope case study was presented and analyzed in FLAC. The cohesion in the upper soil layer was modeled with stationary and non-stationary random fields and the spatial correlation lengths were taken to be isotropic, while the cohesion of the lower rock layer is taken to be deterministic. Results showed the strong effect of the correlation characteristics of the random field on the convergence of the analysis and the probabilities of failure. Figs. 4 and 5 represent stationary and non-stationary random field model (changes with depth) of cohesion for the upper layer and an example of the factor of safety results, respectively.

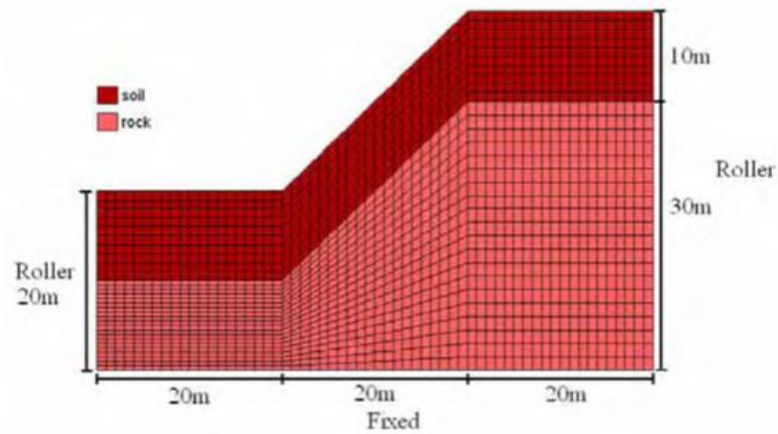


Figure 4. Geometry of Slope Considered in Hong et al. (2016)

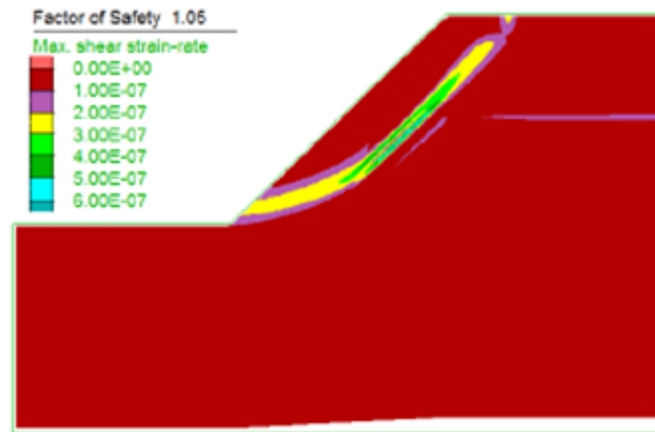


Figure 5. Example of factor of Safety Results (Hong et al., 2016)

Li et al. (2016) also compared previous studies that were based on developments of response surface methods (RSM) using examples of four different slope stability analysis cases. The case analyzed involved (1) single-layered soil slope problem without spatial variability, single-layered soil slope problem considering spatial variability, multiple-layered soil slope problem ignoring spatial variability, and multiple-layered soil slope problem considering spatial variability. Furthermore, the most common RSMs were

compared based on efficiency and accuracy for both cohesive slopes and $c-\phi$ slopes for the aforementioned slope stability cases. Fig. 6 displays a sample of comparison charts for multi-layered cohesive slope with no inherent spatial variability (ISV) and inherent spatial variability while Fig. 7 represents a realization of random field with ISV. The results demonstrated that the efficiency of the RSM depends on the system of soil slope engaged in, where each RSM is best employed for a certain slope stability case. Nevertheless, when including spatial variability for either single or multiple layered system, the multiple stochastic response surface method (MSRSM) proved to be the most efficient method.

Methods	Equivalent number of performance function evaluations of each run	Mean value of P_f	COV[P_f]	Unit COV	Methods	Equivalent number of performance function evaluations of each run	Mean value of P_f	COV[P_f]	Unit COV
SQRSM	7.05	0.216	0.002	0.005	SQRSM	5029.43	0.027	0.03	2.34
MQRSM	15.61	0.184	0.002	0.009	MQRSM	5033.10	0.057	0.02	1.43
SSRSM	10.04	0.219	0.534	1.694	SSRSM	800.08	0.088	0.08	2.19
MSRSM	15.37	0.240	0.522	2.047	MSRSM	801.50	0.031	0.02	0.69
MCS	100.00	0.197	0.095	0.952	MCS	1000.00	0.057	0.08	2.54

Figure 6. Results obtained from three-layered cohesive slope for no ISV and ISV respectively (Li et al., 2016)

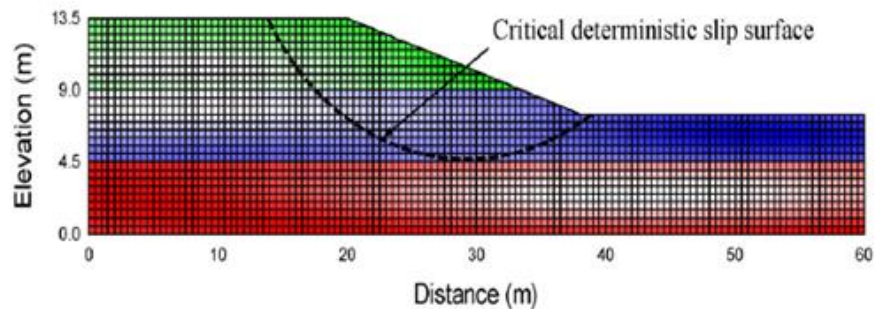


Figure 7. Realization of random field with ISV (Li et al., 2016)

Zaskórski et al. (2017) presented a stochastic analysis of bearing capacity of a shallow foundation on a two-layered soils. Soil strength parameters (friction angle and

cohesion) were characterized as random fields and computations were modeled by RFEM. Cases analyzed presented variations of strong and weak layers configurations, layers thicknesses, correlations lengths and COV's. Results indicated dependency of the stochastic bearing capacity of shallow foundations on the stochastic characterization of soil parameters in the two layers.

Liu et al. (2017) addressed the effect of stratigraphic boundary uncertainty in spatially variable layered slopes on the system reliability. The spatial variability of soil strength properties is simulated by non-stationary random fields and the stochastic stratigraphic boundary is simulated by discrete random variable. Reliability analyses for calculating the failure probabilities were conducted using Monte Carlo simulations. Results showed the significance of the role of the stratigraphic boundary uncertainty in determining the slope failure mechanism, and that ignoring this uncertainty would lead to overestimating the slope failure risk except at small coefficients of variation of the friction angle, where the results are underestimated. Fig. 8 represents typical realizations of random fields for soil cohesion and friction angle, while Fig. 9 shows the influence of COV and vertical scale of fluctuation on the probability of failure.

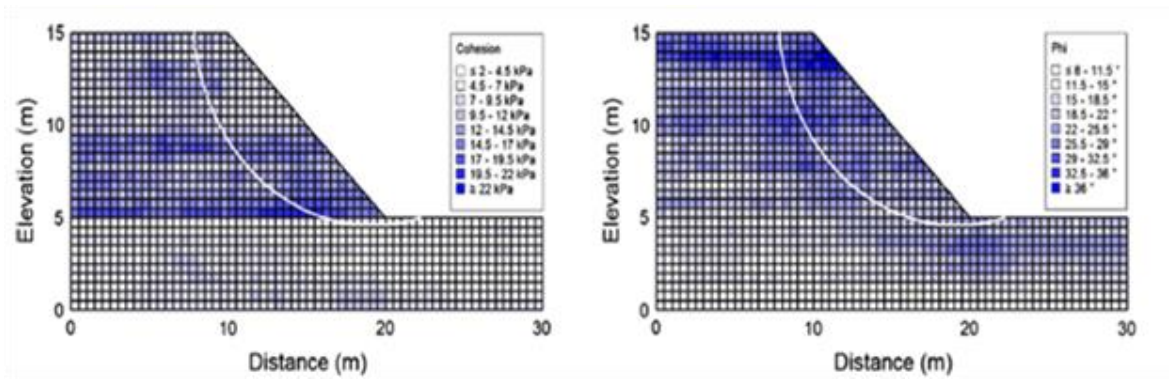


Figure 8. Random Field Realization for Soil properties (Liu et al., 2017)

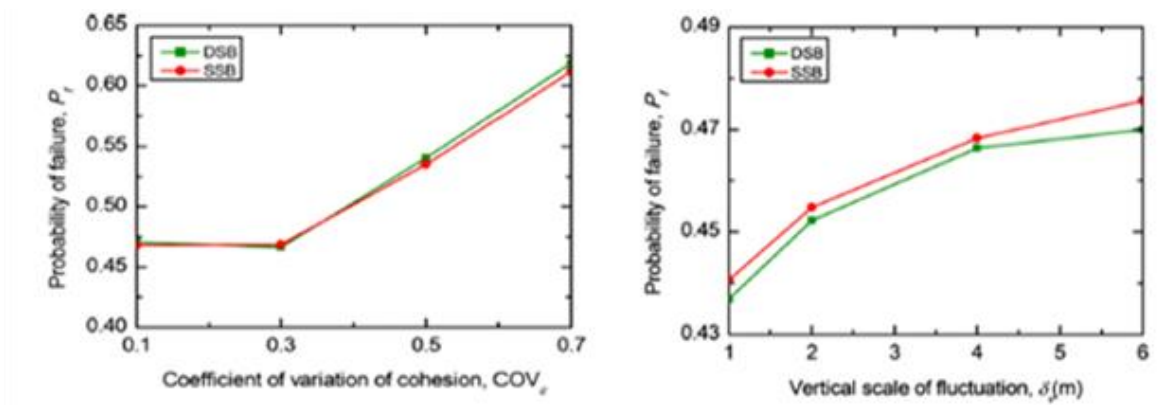


Figure 9. Effect of COV and SOF on probability of failure (Liu et al., 2017)

Finally, Jiang et al. (2017) proposed an approach for risk assessment of slope failure taking into account the spatial variation in soil properties using LEM framework. Using the approach, the slope key failure modes can be identified and their involvement in the slope failure risk is quantified. A two-layered slope is used to illustrate the effectiveness of the approach. The upper shear strength ranged from 80 to 120 kpa, while the lower shear strength ranged from 120 to 160 kpa respectively with a constant COV of 0.3, and a range of correlation lengths for comparison purposes. Fig. 10 shows the effect of correlation lengths on the risk of slope failure for the proposed approach and limit-analysis based

MCS. Results indicated that the proposed approach showed more efficiency than the RFEM by assessing slope failure at small probabilities of failure. In addition, it was concluded that failure surfaces with the highest probability of failure are not necessarily the ones contributing the most to the risk of slope failure.

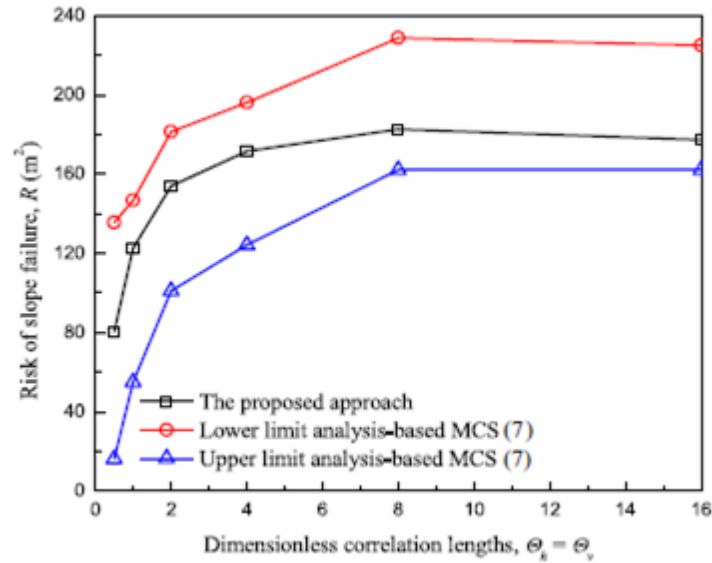


Figure 10. Effect of Correlation Length on risk of slope failure for the proposed approach and the limit analysis-based MCS (Jiang et al., 2017)

CHAPTER III

FLAC SOFTWARE

A. Background

FLAC (Fast Lagrangian Analysis of Continua) is a two-dimensional, explicit finite difference numerical program for engineering mechanics computation that offers a wide range of capabilities to solve complex problems. Typical problem applications that can be treated in FLAC involve mechanical loading capacity and deformations as slope stability and foundations design, tunnel design, soil nailing, earthquake engineering, and liquefaction phenomena in foundations. FLAC was originally developed for geotechnical and mining engineers in 1986 and since then, it has become an essential analysis and design tool in a variety of civil, mining, and mechanical engineering fields. Since its first commercial release in February 1986, it has undergone two major upgrades and subsequently has been updated to the latest version of FLAC 8.0 on December 2015. FLAC is not a black box that will give the solution, since the behavior of the numerical system must be analyzed and interpreted. It is based on a “Lagrangian” calculation scheme that is well suited for modeling large distortions and material collapse.

FLAC also contains a powerful built-in programming language, FISH (short for FLAC-ish), that enables the user to define new variables and functions and offers a unique capability to users who wish to tailor analyses to suit their specific needs. FISH functions were used extensively in this research to map specific soil property values to elements accordingly as will be detailed later.

Materials in FLAC are represented by elements within a grid that is adjusted by the user to fit the shape of the object to be modeled. Each element behaves according to a prescribed linear or non-linear stress/strain law in response to applied forces or boundary restraints. The software takes into account different soil properties as input parameters and the number of realizations in each case is determined from the FISH functions. For each realization, FLAC draws the slope geometry, assign mesh and properties, and then calculates the corresponding factor of safety. The yielded factors of safety of each realization are saved in a separate file. The details of this process are further elaborated in Section 3.

B. Input Parameters

The main input parameters in FLAC are defined and discussed below according to Itasca software guide.

1. Slope Generation

Slope shapes are created using slope tools where the rise with the slope degree, or the rise with the run are determined in addition to the depth and boundary lengths. In this thesis, three slope cases are considered: a slope of angle 30°, angle 45°, and angle 60°. The slope height or rise (H) is taken as 5m or 10m and the total height (d) is taken according to d//H values which will be discussed later in Chapter IV.

2. Finite Difference Grid/Mesh

The finite difference grid is an assemblage of one or more finite difference zones across the physical region that is being analyzed. A grid is defined by specifying the

number of zones “i” desired in the horizontal (x) direction, and the number of zones “j” in the vertical (y) direction. The grid is organized in a row-and-column fashion. Any zone in the grid is uniquely identified by a pair of i, j indices. The mesh sizes chosen are either medium (60 average total zones in the horizontal direction) or fine (100 average total zones in the horizontal direction). The mesh sizes were specified for each case according to a maximum element size of 1m in the vertical direction. Fig. 11 shows an example of fine meshed slope geometry.

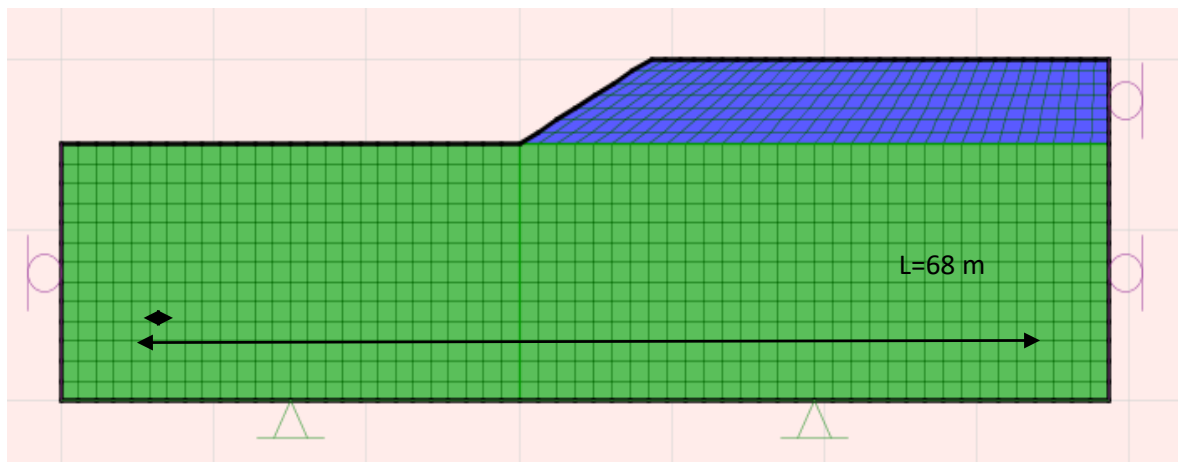


Figure 11. Medium Mesh Slope Geometry

3. *Finite Difference Zone/Element*

The finite difference zone is the smallest geometric domain within which the change in phenomenon can occur. FLAC uses Quadrilateral zones and internally it divides each zone into four triangular “subzones,” but the user is not normally aware of these.

4. *Boundary Conditions*

A boundary condition is the constraint or controlled condition along a model. Automatic boundary conditions are assumed for all slope models of this thesis: roller boundary conditions are applied along the sides of the grid and a fixed (pinned) boundary condition is applied along the bottom.

5. *Number of Realizations*

Each realization in the Monte Carlo process involves the same characteristics of the soil properties; however the spatial distribution varies from one realization to another. A sufficient number of realizations is required for the results to be accurate. The number of realizations N to get a certain degree of precision (indicated by the % error) with 95% confidence is described below:

$$N = \left(\frac{196}{\% \text{ Error in } \mu_Y} \right)^2 \delta_Y^2 \quad (\text{Eq. 3.1})$$

Where % Error in μ_Y is the desired precision in the estimate of mean of Y and δ_Y is the estimate of coefficient of variation of Y . For instance, the number of realizations required in this study for a % Error in μ_Y of 2.5 and a δ_Y of 0.5 (highest possible value) is:

$$N = \left(\frac{196}{2.5} \right)^2 * 0.5^2 = 1536 \text{ realizations} \approx 1500 \text{ realizations}$$

In this study and for further accuracy, runs with 1500 realizations and 5000 realizations were both applied and compared. The results show similar means of factors of safety, which confirms the choice of 1500 realizations as the standard number of N throughout the research.

6. Constitutive Model

The model used in the analysis is the Mohr-Coulomb model, which is the conventional model used to represent shear failure in soils and rocks. The failure envelope for this model corresponds to a Mohr-Coulomb criterion (shear yield function) with tension cutoff (tensile yield function).

7. Strength Reduction

The analysis of slope stability problems in *FLAC* is performed by calculating the factors of safety. The factor of safety is calculated based on the “strength reduction method”. This method has been extensively used as a numerical method for evaluating factor of safety in geomechanics, and it has been commonly applied in the context of Mohr-Coulomb failure criterion. Typically, numerical analyses programs utilizes three different computational methods in calculating the factor of safety for slopes: strength reduction method, limit analysis (upper and lower bound solutions), and limit equilibrium method (upper-bound solution).

The “strength reduction technique” is the most popular method among the others applied, as it calculates the factor of safety by progressively reducing the shear strength of the material to bring the slope to a state of limiting equilibrium.

In this case, the safety factor F is defined according to the Eq. 3.2 and 3.3:

$$c^{trial} = \frac{1}{F^{trial}} c \quad (\text{Eq. 3.2})$$

$$\phi^{trial} = \arctan\left(\frac{1}{F^{trial}} \tan\phi\right) \quad (\text{Eq. 3.3})$$

A series of simulations are made using trial values of the factor F to reduce the cohesion, c , and friction angle, ϕ , until slope failure occurs. One technique to find the strength values that correspond to the onset of failure is to monotonically reduce (or increase) the strengths in small increments until a failure state is found. Alternatively, in *FLAC*, a bracketing approach similar to that proposed by Dawson, Roth and Drescher (1999) is used. With this technique, stable and unstable bracketing states are found first, and then the bracket between the stable and unstable solution is progressively reduced until the difference between stable and unstable solutions falls below a specified tolerance.

8. *Spatial Correlation*

Generally, soil particles at adjacent locations share more similar parameters than those at remote locations (Li et al., 2015). This phenomenon is what is known as spatial variability of soil properties, and it is governed by the autocorrelation coefficient functions (ACF) between the parameters at any two points. Typically, theoretical ACFs are assumed in research due to the limited site investigation data. In other words, the correlation length corresponds to the distance between two points where soil parameters are assumed to be correlated. Therefore, spatial variation in soil properties is significantly represented in the correlation structure (Vanmarcke 1983).

Assuming a large autocorrelation distance value means the soil property is highly correlated for a large spatial distance. However, assuming a small autocorrelation distance implies that the soil property has large fluctuations through the soil (Cho, 2010). For clarification, taking a correlation length of 10 m implies that any two soil points within a distance less than 10 m will have correlated soil properties. On the other hand, if the

distance between these two points was more than 10 m, they would have statistically independent soil properties.

In the geotechnical field, the uncertainty in soil properties is typically modelled through the lognormal distribution (ex. undrained strength S_u) and the spatial correlation length is commonly measured by the correlation distance for $\ln s_u$ instead of s_u , since the logarithm of the lognormal distribution yields a Gaussian (normal) distribution. This spatial correlation length ($\theta_{\ln s_u}$) defines the distance beyond which the spatially random values of S_u will no longer be correlated in the normal field. Therefore, a large value of the correlation length ($\theta_{\ln s_u}$) represents smooth variation across the field, while a small value represents a more abrupt field with little correlations. The spatial correlation length is calculated after performing statistical analyses of shear strength data. The magnitude of the spatial correlation length estimated in the Gaussian field doesn't vary much from the correlation length in the real space of S_u and therefore $\theta_{\ln s_u}$ and θ_{s_u} are interchangeable given their inherited uncertainty (Griffiths and Fenton, 2004).

In this paper, a Markovian correlation function that is exponentially decaying is used (Griffiths and Fenton 2004) as indicated in Eq. [3.4]:

$$\rho = e^{-2\tau / \theta_{\ln s_u}} \quad (\text{Eq. 3.4})$$

Where ρ is the correlation coefficient assumed between two points and τ is the absolute distance between two points in a random field. According to Griffiths and Fenton (2004), this correlation form will give a correlation value of 0.135 for a distance between two points equal to $\theta_{\ln s_u}$. For smaller distances, the correlation ρ increases and therefore,

this correlation function serves as a way to reflect the field observation that soil samples taken close together are more likely to have similar properties than samples taken far apart. As a result, fields with large correlation lengths (θ_{Incu}) are considered smooth, unlike fields with small correlation lengths which are considered to be erratic and unpredictable.

In the geotechnical literature, it is often assumed that soil properties follow an isotropic correlation structure. In fact, correlations in the vertical direction exhibit shorter distances than those in the horizontal direction. In other words, soils tend to exhibit anisotropy where the spatial correlation lengths for c_u vary for each orthogonal direction (horizontal and vertical), whereby the lateral or horizontal direction demonstrates longer correlation lengths with respect to the vertical direction, since the soil is layered horizontally. This means there will be slower variations in the soil properties across the horizontal direction. This anisotropy correlation is attributed to the process of geological soil formation and post depositional history that characterizes most natural soil deposits (Cho et al., 2010). According to Cherubini (1997) and Phoon and Kulhawy (1999), typical values for horizontal scales of fluctuation range from 30 to 60m and from 1 to 3m for vertical scales of fluctuation.

To account for anisotropy in the correlation structure, the anisotropic autocorrelation model shown in Eq. 3.5 is generally adopted (Jha and Ching 2013):

$$\rho(\Delta x, \Delta z) = \exp\left(-\frac{2|\Delta x|}{\delta_x} - \frac{2|\Delta z|}{\delta_z}\right) \quad (\text{Eq. 3.5})$$

Where δ_x and δ_z are the horizontal and vertical correlation lengths respectively, and Δx and Δz are the horizontal and vertical distances between two points in space.

Figs. 12 and 13 show two illustrations of slopes with isotropic random fields of S_u with $\delta=40\text{m}$ and $\delta=2\text{m}$ in both directions respectively. The examples relates to a slope with an angle= 30° , $H=5\text{m}$, and $d/H=3$ with mean $c_{u1}=100\text{ kPa}$, mean $c_{u2}=20\text{ kPa}$ and COV $c_u=0.5$. Fig. 13 shows that the colors which represent different ranges of S_u values change more frequently than Fig.12 where colors vary more smoothly. The rapid change observed reflects the small correlation length assigned to the slope. As the correlation length increases, the change in the shear strength values for the elements becomes less abrupt and slower.

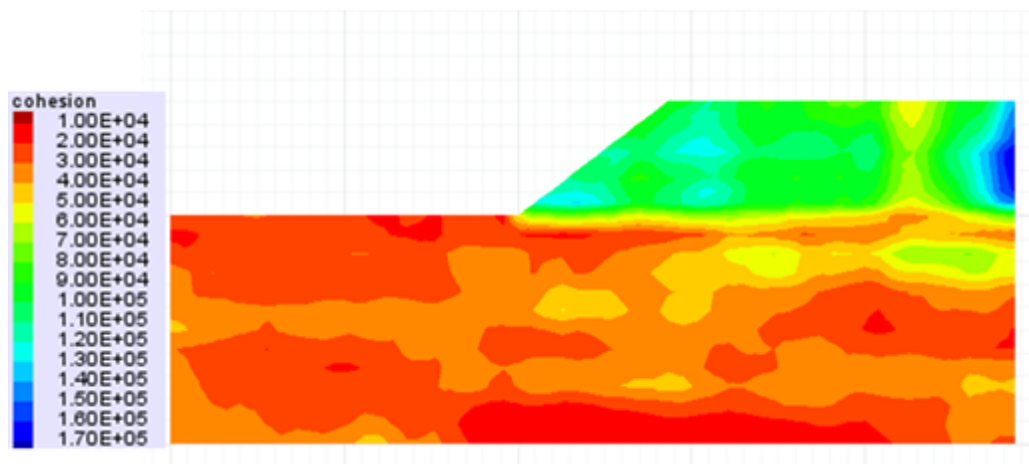


Figure 12. Realization with isotropic random field $\delta=40\text{m}$

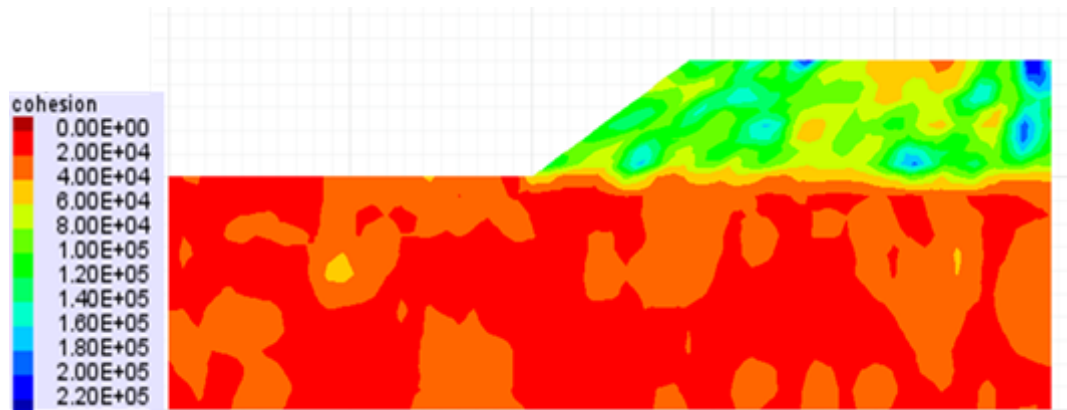


Figure 13. Realization with isotropic random field $\delta=2\text{m}$

Fig. 14 shows the same slope but for anisotropic random field with $\delta_x=40\text{m}$ and $\delta_y=2\text{m}$. In the isotropic structure with $\delta_x=\delta_y=2\text{m}$ (Fig. 14 (a)), the variation in the undrained shear strength values along both the vertical and horizontal directions was very rapid. On the contrary, Fig. 14 (b), which reflects the anisotropic case with $\delta_x=40\text{m}$ and $\delta_y=2\text{m}$, shows smoother variation in the horizontal direction which is due to the higher correlation length assigned in this direction.

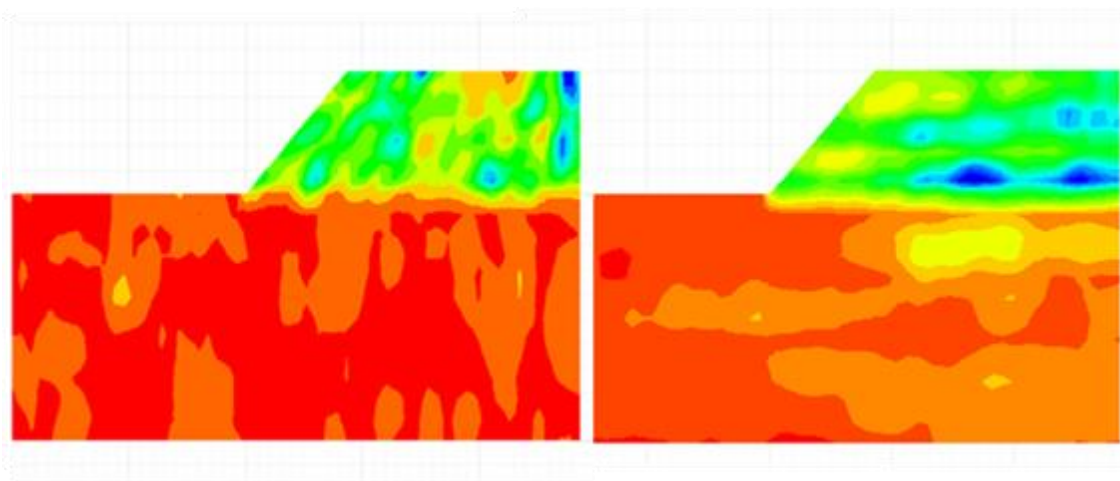


Figure 14. Realization with (a) isotropic random field $\delta_x = \delta_y = 2\text{m}$ and (b) anisotropic random field with $\delta_x = 40\text{m}$ and $\delta_y = 2\text{m}$

9. Friction Angle

The friction angle is taken to be zero since the research analyzes slopes made of undrained clayey soil.

10. Elastic Modulus

The elastic modulus defined as the ratio of stress over strain is taken to be deterministic with a value of 40,000 kPa.

11. Poisson's Ratio

The Poisson ratio is taken as deterministic with a magnitude of 0.45.

12. Mass Density

The mass-density which is the unit weight of the soil is also taken as deterministic with a value of 20 KN/m³ or 2039 Kg/m³ for the upper layer and 18 KN/m³ or 1835 Kg/m³ for the lower layer.

C. Probabilistic Distribution of Shear Strength

1. Lognormal Distribution

In this study, the undrained shear strength is expected to be the source of uncertainty while all other soil parameters are taken to be deterministic. For all of the cases, S_u is characterized statistically by a log-normal distribution which is defined by a mean, μS_u , and a standard deviation σS_u following the model described by Griffiths and Fenton (2004). The probability density function (PDF) of a log-normal distribution is described in Eq. 3.6 below:

$$f(S_u) = \frac{1}{S_u \sigma_{\ln S_u} \sqrt{2\pi}} e^{-\frac{1}{2} \left(\frac{\ln S_u - \mu_{\ln S_u}}{\sigma_{\ln S_u}} \right)^2} \quad (\text{Eq. 3.6})$$

The mean and the standard deviation of the lognormal distribution are related by the dimensionless coefficient of variation COV, and are expressed in Eq. 3.7:

$$\text{COV} = \frac{\sigma_{S_u}}{\mu_{S_u}} \quad (\text{Eq. 3.7})$$

The standard deviation and mean underlying normal distribution are defined in Eq 3.8 and 3.9 as follows:

$$\sigma_{\ln S_u} = \sqrt{\ln \left\{ 1 + \left(\frac{\sigma_{S_u}}{\mu_{S_u}} \right)^2 \right\}} \quad (\text{Eq. 3.8})$$

$$\mu_{\ln S_u} = \ln \mu_{S_u} - \frac{(\sigma_{\ln S_u})^2}{2} \quad (\text{Eq. 3.9})$$

Rearranging Eq. 3.8 and 3.9 above yields the mean and the standard deviation of the lognormal distribution as shown in Eq. 3.10 and 3.11:

$$\mu_{S_u} = \exp\left(\mu_{\ln S_u} + \frac{1}{2} \sigma_{\ln S_u}^2\right) \quad (\text{Eq. 3.10})$$

$$\sigma_{S_u} = \mu_{S_u} \sqrt{\exp(\sigma_{\ln S_u}^2) - 1} \quad (\text{Eq. 3.11})$$

2. Local Averaging

In the finite element analysis, simulating single S_u values for each element is more important than simulating the random field $S_u(x,y)$ within each element (Jha and Ching, 2013). According to Griffiths and Fenton, this can be corrected by the use of local averaging and consideration of the sample size (Griffiths and Fenton, 2004).

For the case where the point distribution is a normal distribution, local averaging has shown to affect the variance of the property by reducing the variance but not the mean. However, for lognormal cases, it has shown to reduce both the standard deviation and the mean. This behavior was explained by Griffiths and Fenton due to the dependence of the mean of the lognormal distribution on the mean and variance of its normal distribution.

The variance reduction factor due to local averaging γ , is defined as (Griffiths and Fenton, 2004):

$$\gamma = (\sigma_{\ln S_{uA}} / \sigma_{\ln S_u})^2 \quad (\text{Eq. 3.12})$$

Where $\sigma_{\ln S_{uA}}$ is the standard deviation of the average soil property.

Spatial averaging is affected by the scale of fluctuation and the length of the averaging interval, which is the approximate length of the failure surface. Vanmarcke (1983) discussed the concept of variance reduction as the result of spatial averaging of soil properties. The effect of the variance reduction process decreases the variance of the random field used to model the spatial variability in the soil property and therefore reduces the uncertainty in this soil property. This process is known to occur when the length of the failure surface (averaging length) is larger than the correlation length which defines the

scale of fluctuation of the soil property. Results show that the impact of variance reduction becomes more significant when the correlation length approach the element size (Farah et al. 2016). The approximate variance reduction function defined according to Vanmarcke (1983) is shown below:

$$\Gamma^2 = 1 \quad \text{for } L_a \leq \delta_v \quad (\text{Eq. 3.13})$$

$$\Gamma^2 = \frac{\delta_v}{L_a} \quad \text{for } L_a > \delta_v \quad (\text{Eq. 3.14})$$

where: δ_v = vertical scale of fluctuation and L_a = averaging interval.

In this study, since the size of each element is approximately 1m in both directions, the variance reduction effect will be more significant for $\delta = 1\text{m}$.

3. Generating & Mapping of Random Fields

To generate the random field of undrained shear strength c_u , R software and Microsoft Excel were used in this study. The main input parameters for the code in R are the statistical parameters of the shear strength distribution for the two layers (mean and COV), the correlation length in the horizontal and vertical direction, the coordinates of the elements taken from the slope geometry drawn in FLAC, the depth of each layer and the number of realizations. The procedure for generating and mapping the undrained shear strength random field into their respective elements is described in the following steps:

(1) Slope geometry is drawn in FLAC with the proper meshing ensuring all conditions are met (boundary and element size).

(2) The deterministic factor of safety is calculated and the length of the failure surface is measured in AutoCAD.

(3) The coordinates of the elements making up the slope geometry are exported from FLAC into notepad files through the FISH function below:

```
def_expo
loop m(1,88)
m=m+1
loop n(1,44)
n=n+1
aa=x(m,n)
bb=y(m,n)
cc= out(string(aa) +' ' + string(bb))
end_loop
end_loop
end
_expo
```

(4) The coordinates are transferred into Excel worksheets and called in R as an input parameter.

(5) After filling all input parameters required by R, the random field of the undrained shear strength is generated for the number of realizations required in the form of two Excel worksheets for each of the two layers, as detailed in the following steps:

a) Define the input parameters for the two layers and call the Excel file of the slope elements coordinates.

```
iy=4      #Y-coordinate of the interface between layers
clx1=40   #Horizontal correlation length of layer 1 (top)
cly1=4    #Vertical correlation length of layer 1 (top)
clx2=40   #Horizontal correlation length of layer 2 (bottom)
cly2=4    #Vertical correlation length of layer 2 (bottom)
nr=1500   #Number of realizations/simulations
msu1=100  #Mean of undrained shear strength of layer 1
covsu1=0.4 #cov of undrained shear strength of layer 1
msu2=50   #Mean of undrained shear strength of layer 2
```

```

covsu2=0.4 #cov of undrained shear strength of layer 2
da=(read.csv("F:/FLACfile/PART Two/Uncertain Cases-Angle 45/Case 262/geometry1.csv"))
da=data.frame(N=seq(1,length(da[,1]),1),X=da[,1],Y=da[,2])

```

b) For each layer, calculate the distance between any two elements by constructing dx and dy matrices.

```

#Layer 1(top)
da1=da[da$Y>=iy,]
#constructing dx and dy matrices for layer 1
dx1=matrix(rep(NA,length(da1$X)^2),length(da1$X),length(da1$X))
dy1=matrix(rep(NA,length(da1$X)^2),length(da1$X),length(da1$X))
for (i in 1:length(da1$X)){
  for (j in 1:length(da1$X)){
    dx1[i,j]=abs(da1$X[i]-da1$X[j])
    dy1[i,j]=abs(da1$Y[i]-da1$Y[j])
  }
}

```

c) Construct the correlation matrix based on the markovian function in Eq. 3.4.

```

#Constructing Correlation matrix for layer 1
cormat1=exp(-(2*dx1/clx1+2*dy1/cly1))
isSymmetric(cormat1)

```

d) Generate correlated random variables that belong to the standard normal distribution (with mean=0 and std=1) and then transfer them into a uniform distribution.

```

AB1 <- rmvnorm(mean=rep(0,length(da1$X)),sig=cormat1,n=nr) #Our gaussian variables
U1 <- pnorm(AB1) #Now U is uniform - check using hist(U[,1]) or hist(U[,2])

```

e) Define the mean and standard deviation of the lognormal distribution to be generated and build an empty matrix with the proper dimensions to transfer the uniform distribution into a lognormal distribution.

```

sdsulog=sqrt(log(1+covsu1^2))
msulog=log(msu1)-sdsulog^2/2
UU1=matrix(rep(NA,I(length(da1$X)*nr)),nr,length(da1$X))
for (i in 1:length(da1$X)){
  UU1[,i]=qtrunc(U1[,i],spec="lnorm",a=0,b=Inf,msulog,sdsulog)
}

```

f) Transfer the generated random variables into an Excel worksheet, and calculate the exact mean and standard deviation for the 1500 realizations generated.

```
write.csv(t(UU1), "F:/FLACfile/PART Two/Uncertain Cases-Angle 45/Case 262/realization1.csv")
```

```
rmax=rep(NA,nr)
rmin=rep(NA,nr)
rmean=rep(NA,nr)
for (i in 1:nr){
  rmax[i]=max(UU1[i,])
  rmin[i]=min(UU1[i,])
  rmean[i]=mean(UU1[i,])
}
max(rmax)
min(rmin)
mean(rmean)
```

(6) Use Visual Basic in Excel to distribute the c_u values of each realization into separate notepad files.

```
Sub Do_itt()
  Dim fs As Object
  Set fs = CreateObject("Scripting.FileSystemObject")
  For c = 1 To 16000
    fn = Cells(1, c)
    Set a = fs.CreateTextFile("F:\FLACfile\PART Two\Uncertain Cases-Angle 60\Case 208\" & fn & ".txt",
True)
    r = 2
    While Not IsEmpty(Cells(r, c))
      a.writeline Cells(r, c)
      r = r + 1
    Wend
  Next c
End Sub
```

(7) A master function is called in FLAC, where it calls another FISH function inside it. These functions are repeated according to the number of realizations required. The functions are responsible for drawing the slope geometry, mapping the shear strength value for the corresponding realization to each element, running the model to calculate the factor of safety, and storing it in a common notepad file.

```
new  
call 01_Lib.dat  
set cohesion_filename= 'V1.txt'  
set cohesion_filename= 'J1.txt'  
call 02_run.dat  
call factorof.dat
```

For more details, the full codes and FISH functions used in the process described above are shown in Appendix A.

CHAPTER IV

DETERMINISTIC ANALYSIS OF MULTI-LAYERED CLAYEY SLOPES

A. Slope Parameters

In this chapter, results from FLAC stability analyses that were conducted on several slope geometries and soil parameters for two-layered slope models will be presented and analyzed. The cases that will be considered involve a stiff upper layer resting on a softer lower layer, which is in turn assumed to be underlain by bedrock (Figure 15). The slope is assumed to be located entirely in the upper stiff layer. The undrained shear strength of the upper layer (c_{u1}) was assumed to be of a constant value of 100 Kpa, and the undrained shear strength of the lower layer (c_{u2}) was varied depending on three ratios for $c_{u1}/c_{u2}=1.5, 3,$ and 5 . To simulate slope cases that reflect practical scenarios in the field, the slope height (H) was chosen to be either 5m or 10m with the base case being considered as $H= 5$ m. The thickness of the second layer was varied depending on four d/H ratios (1.5, 2, 3, and 5), where H represents the thickness of the first layer (slope height) and d represents the cumulative thickness of both layers (Figure 15).

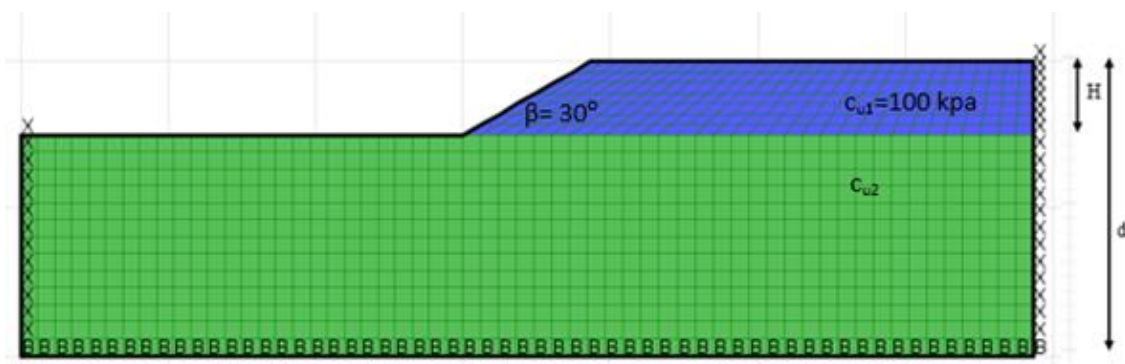


Figure 15. Slope geometry in FLAC

The slope system presented in Figure 15 models practical cases of two-layered clayey slopes, whereby the slope is usually comprised of compacted stiff clay or a natural cut in a desiccated crust that is over consolidated due to seasonal geologic fluctuations in the level of the water table. According to Mwasha (2011), the thickness of desiccated crusts generally varies between 1 and 3 meters, and may go up to maximum depths of 6 to 7m. These considerations dictated the choice of a slope thickness of $H = 5\text{m}$ for the base case analyzed in this study. To account for the effect of the slope inclination, slope cases with three slope angles ($\beta=30^\circ$, 45° , and 60°) were analyzed. As a result, the major parameters that were varied in the deterministic analysis are: (1) c_{u1}/c_{u2} , (2) d/H , and (3) β . For the probabilistic analysis, additional parameters are considered as will be discussed in Chapter V.

B. FLAC Stability Results

In the deterministic stability analyses that were conducted in FLAC, the undrained strengths in both layers were assumed to have deterministic constant values. Thirty six deterministic stability analyses ($c_{u1}/c_{u2} = 1.5, 3.0$ and 5.0 , $d/H = 1.5, 2.0, 3.0$, and 5.0 , and $\beta = 30, 45$, and 60 degrees) were performed to investigate the effect of the different parameters on the deterministic factor of safety (FS) and the stability factor (N). The factor of safety FS was determined directly from the output of FLAC, while the dimensionless stability number N was calculated according to Eq. 3.15 such that:

$$N = \frac{c_{u1}}{\gamma * H * FS} \quad (\text{Eq. 3.15})$$

Where c_{u1} is the undrained shear strength of the top layer (KN/m^2), γ is the unit weight of the top layer (KN/m^3), H is the slope height or the thickness of the top layer (m) and FS is

the calculated factor of safety. The stability number N was first proposed by Taylor (1937) to normalize the factor of safety with the respect to the undrained shear strength value assigned for the top layer (c_{u1}) and the slope height (H) as will be further elaborated in section C.

The deterministic stability number N_d that was calculated using FLAC for the 36 deterministic cases analyzed in this study is plotted on Figure 16 as a function of the d/H ratio for slopes with different inclination angles and different ratios of c_{u1}/c_{u2} . The results on Figure 16 indicate that N_d is highly dependent on the ratio c_{u1}/c_{u2} , and less sensitive to β and d/H . For any given slope angle and geometry, N_d increases as c_{u1}/c_{u2} increases. This relationship is expected given that large c_{u1}/c_{u2} ratios are indicative of a softer lower clay layer. A softer clay layer results in a reduction in the factor of safety which in turn results in an increase in the value of N_d (see Equation 3.15). The sensitivity of N_d to the ratio c_{u1}/c_{u2} increases for larger d/H ratios, since the effect of the soft lower clay layer on the factor of safety becomes more significant when the soft layer is thick relative to the upper stiff layer (larger d/H). If c_{u1}/c_{u2} is held constant, results on Figure 16 clearly indicate that the stability number increases as d/H increases (thickness of soft layer increases). As expected, this effect becomes negligible for the smallest c_{u1}/c_{u2} considered (low contrast between shear strength of two layers) and increases for the largest c_{u1}/c_{u2} considered (Figure 16). As an example, for the case of $c_{u1}/c_{u2}=5$, N_d is found to increase from 0.59 to 0.91 as d/H increases from 1.5 to 5. This increase is less pronounced for $c_{u1}/c_{u2}=1.5$, where N_d increases from 0.23 to 0.28 as d/H increases from 1.5 to 5.

Finally, it is clear on Figure 16 that the angle of the slope β has the smallest effect on the stability number N_d , particularly for cases with large d/H ratios where the stability seems to be governed by the strength of the soft soil layer rather than changes in slope geometry. The effect of β on the stability number starts to become significant at lower d/H ratios, particularly for cases where the contrast between the strength of the stiff clay layer and the soft clay layer is high ($c_{u1}/c_{u2} = 3$ and 5). For these cases, a significant proportion of the failure surface lies in the upper clay layer (small d/H ratios) and the angle of the slope starts to have an influence on the stability number N_d .

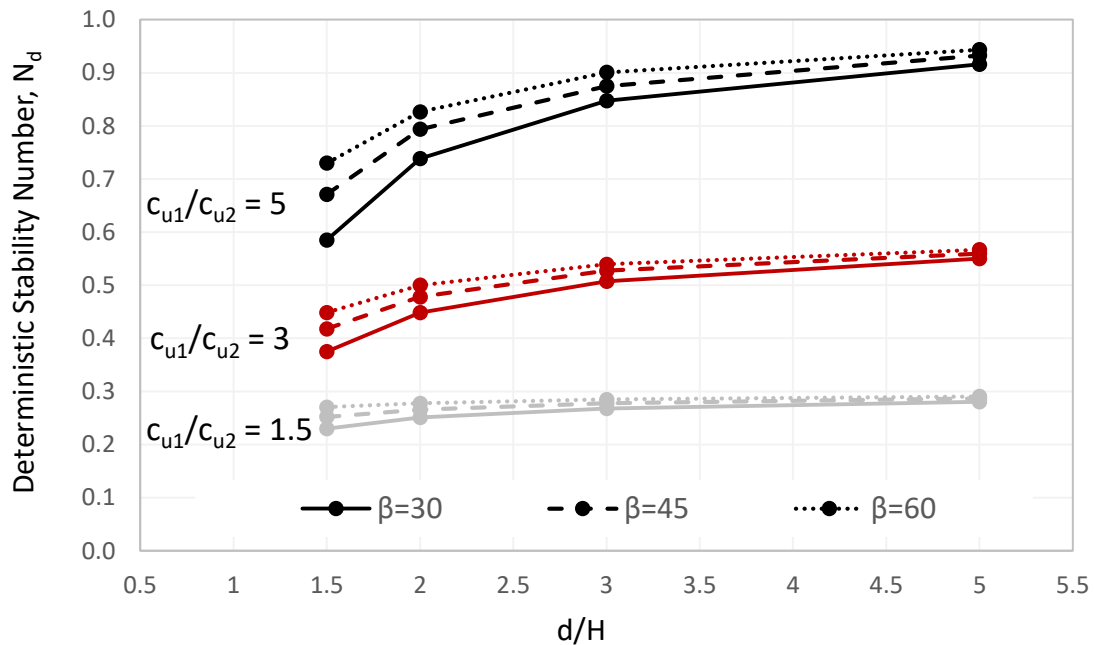


Figure 16. Variation of N_d with respect to d/H , c_{u1}/c_{u2} , and β

To investigate the mechanism of failure in the two-layered slope system for different geometry and strength conditions, the variation of the maximum shear strain increment studied on Figure 17 for representative two-layered slope cases with different

geometric and strength characteristics. The first observation from Figure 17 is that the governing mode of failure is a deep seated/foundation failure, irrespective of the choice of β , d/H , and c_{u1}/c_{u2} . The deep seated failure is expected given the contrast in shear strength between the two layers whereby the soft layer is always at the lower part/foundation of the slope. An investigation of the effect of the c_{u1}/c_{u2} ratio on the failure surface indicates that for cases with large c_{u1}/c_{u2} ratios, the maximum shear strain increments are mostly concentrated in the lower soft layer and the portion of the failure surface that lies in the upper stiff slope is relatively steep.

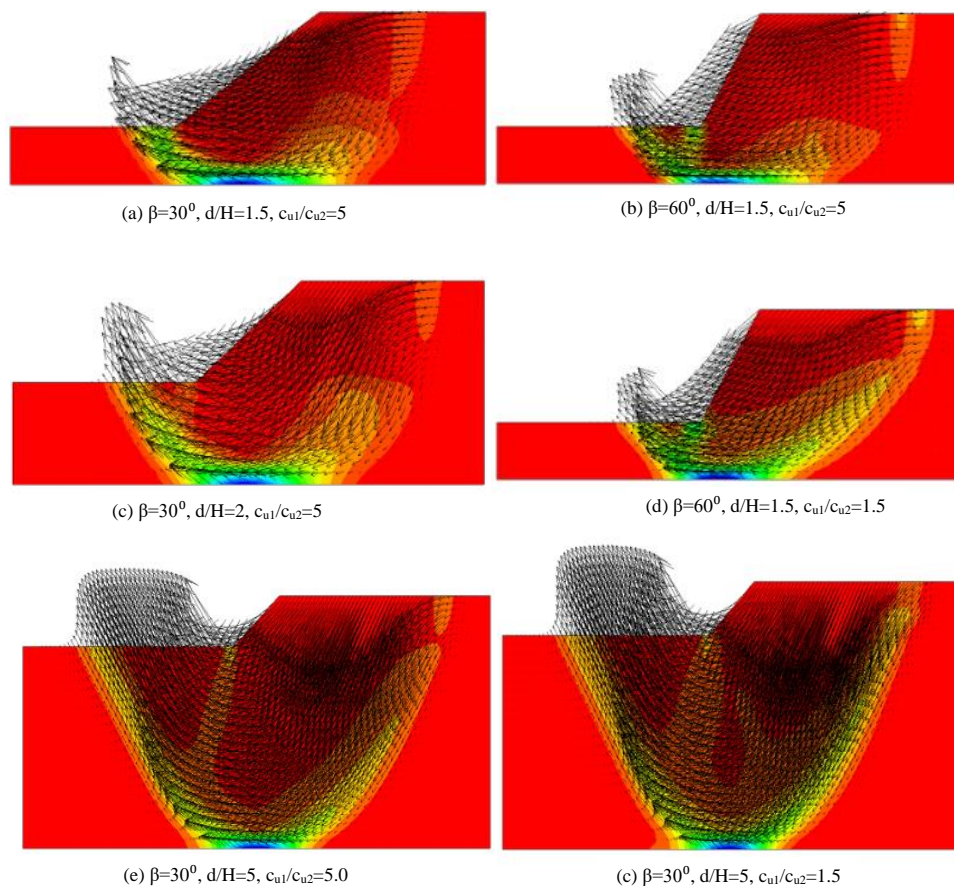


Figure 17. Shadings of the Maximum Shear Strain Increment for samples of the two-layered slope cases analyzed (Shear strain increment increases from red, to orange, to yellow, to green and finally to blue).

C. Effect of the undrained shear strength of the top layer (c_{u1})

The undrained shear strength of the upper layer of the slope (c_{u1}) is taken as a constant value of 100 kpa throughout all the slope models. It is expected that varying the undrained shear strength value should not have an effect on the results of dimensionless stability factor, N although it would definitely affect the resulting factor of safety of any given slope. Taking lower values of the upper undrained shear strength will yield lower factors of safety. However, when calculating N , the effect of a smaller denominator in Equation 3.15 is offset by the low shear strength (c_{u1}) value in the numerator. This should eliminate any effect caused by changing the value of the undrained shear strength of the upper layer on N values particularly for the deterministic analysis. The same logic applies for the opposite cases of higher undrained shear strengths.

To verify this assumption, two cases of higher and lower shear strengths values of the upper layer were considered. The results of N_d for shear strengths values of $c_{u1}=70$ kpa and $c_{u1}=200$ kpa for $\beta=30^\circ$, $d/H=3$ were calculated and compared with the base case of shear strength $c_{u1}=100$ kpa in Table 1. The results of N_m are even compared for the case of random field for future reference. As expected, the results indicate that N_d is almost insensitive to the assumed values of the undrained shear strength in the upper layer with a maximum error of 1.9% in the resulting values of N_d . Based on these results, a decision was made to use a constant value of $c_{u1}=100$ kpa in the balance of this study.

It should be noted however that while the deterministic N_d values was not sensitive to the choice of c_{u1} , this does not guarantee that the probabilistic characteristics of N will not be affected for the cases where the undrained shear strength is assumed to be a

random variable. To get a feeling of whether the mean value of N (N_m) will be sensitive to the choice of c_{u1} , probabilistic analyses were conducted for the same cases presented in Table 1, except that c_{u1} and c_{u2} were assumed to be described by random fields having a coefficient of variation of 0.5 and vertical and horizontal correlation lengths of 2m and 40m, respectively. The analyses were repeated while changing the mean value of c_{u1} from 70 kPa to 200 kPa. The resulting mean values of N are presented in Table 1. Results show that although the mean value of the stability number (N_m) is slightly different than the deterministic value of N (N_d), there is no noticeable impact of the choice of the mean of c_{u1} on the results. These observations confirm the fact that probabilistic runs with a constant value of 100 kPa for the mean of c_{u1} are sufficient to quantify the reliability of the two-layered slope cases analyzed in this study.

Table 1. Sensitivity of the Results of N_d and N_m to the choice of c_{u1}

c_{u1}/c_{u2}	$\beta=30^\circ, d/H=3$			COV $c_u=0.5, \delta_x=40m, \delta_y=2m$		
	$c_{u1}=100$ kpa	$c_{u1}=70$ kpa	$c_{u1}=200$ kpa	$c_{u1}=100$ kpa	$c_{u1}=70$ kpa	$c_{u1}=200$ kpa
	N_d	N_d	N_d	N_m	N_m	N_m
5	0.847	0.843	0.846	1.010	1.014	1.010
4	0.680	0.675	0.676	0.813	0.814	0.810
3	0.508	0.508	0.509	0.621	0.609	0.613
2.5	0.427	0.426	0.427	0.524	0.519	0.519
2	0.348	0.348	0.348	0.427	0.424	0.424
1.5	0.268	0.269	0.268	0.330	0.329	0.329

D. Regression Model for the Deterministic Dimensionless Stability Number (N_d)

The results presented in Figure 16 cover a wide range of cases that could encompass practical problems involving two-layered clayey slopes with a slope comprised of a stiff layer overlying a foundation comprised of a softer layer. These results were used to develop a simplified empirical equation that allows the designer to predict the deterministic dimensionless stability number N_d without the need for running computationally demanding numerical analyses using FLAC. The empirical equation expresses N_d as a non-linear function of β , d/H , and c_{u1}/c_{u2} such that:

$$N_d = 0.141 \cdot \left(\frac{c_{u1}}{c_{u2}}\right)^{0.942} \cdot (\tan \beta)^{0.092} \cdot \left(\frac{d}{H}\right)^{0.245} \quad (\text{Eq. 3.16})$$

The constants in Equation 3.16 were determined using regression based on the deterministic results obtained from FLAC. The mathematical formulation of equation 3.16 is simple and the resulting regression constants point to the significant impact of c_{u1}/c_{u2} and the negligible impact of the slope angle β on the results. These trends are realistic and were discussed in the previous section. To investigate the reliability of the empirical correlation (Eq. 3.16) and its predictive performance for cases that were not included in the calibration data, 20 additional stability runs (Appendix A) for cases that include combinations of β , d/H , and c_{u1}/c_{u2} that are different than those presented in Fig. 16 were analyzed in FLAC. The FLAC-predicted N_d values were obtained and compared with the N_d values predicted from Equation 3.16 on Figure 18. Results indicate that the simple empirical model (Eq. 3.16) is reliable and yields an acceptable predictive performance. To quantify the bias and uncertainty in the simplified model predictions, the ratio (FLAC N_d /Predicted N_d) was calculated for the 20 cases. Results show that the mean of this ratio is 1.02 (model is

unbiased) and the coefficient of variation (COV) is relatively small with a value of 0.03. These statistics indicate that the simplified model could be used with confidence to predict the deterministic values of N_d for a two-layered slope system with parameters that fall in the range of the input parameters used in the FLAC analysis.

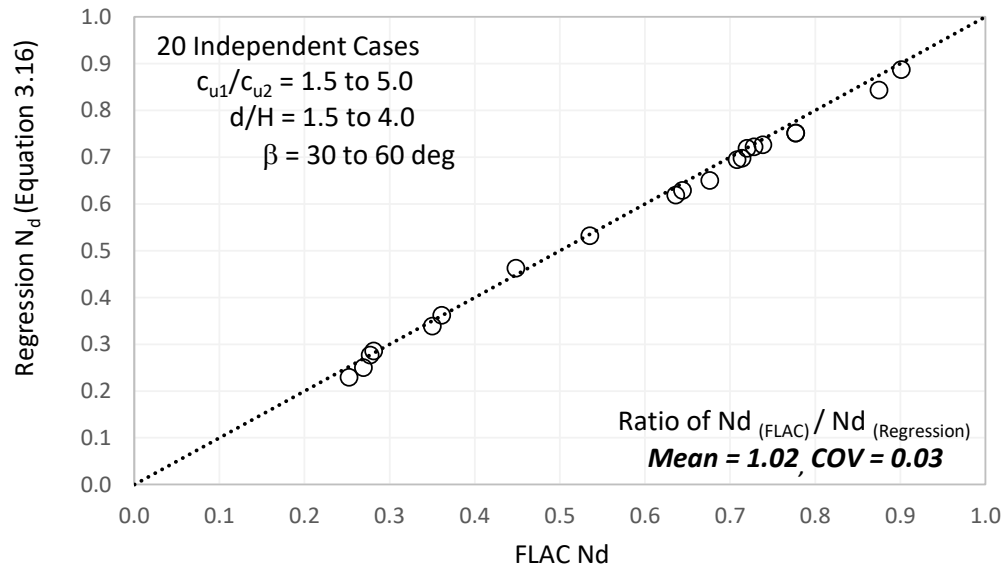


Figure 18. Performance of Regression Model based on 20 Independent Analysis Cases

CHAPTER V

STABILITY RESULTS FOR SPATIALLY VARIABLE TWO-LAYERED CLAYEY SLOPES

A. Introduction

The main objective of this research study is to assess the impact of spatial variability in the undrained shear strength on the probability of failure of two-layered clayey slope systems. The aim is to use robust random field models to model the spatial variability of the clay properties within FLAC and to establish simplified relationships between the deterministic factor of safety and the probability of failure of the slope system. The major parameters that will affect the reliability of the slope are c_{u1}/c_{u2} , d/H , and β , in addition to the probabilistic characteristics of the random field of c_{u1} and c_{u2} . To simplify the analysis, the coefficient of variation of the undrained shear strength is assumed to be the same for both layers with assumed values of 0.3 and 0.5. The vertical scale of fluctuation (δ_y) is assumed to vary between 1, 2, and 5m while the horizontal scale of fluctuation (δ_x) is assumed to be constant at a value of 40m. Assuming the same properties of the random field of the undrained shear strength in the two layers can be considered a limitation in this study. This assumption could be relaxed in future studies. Fig. 19 shows the slope geometry with the main parameters that are varied in the probabilistic analysis in an attempt to determine empirical models that relate between the deterministic and probabilistic results.

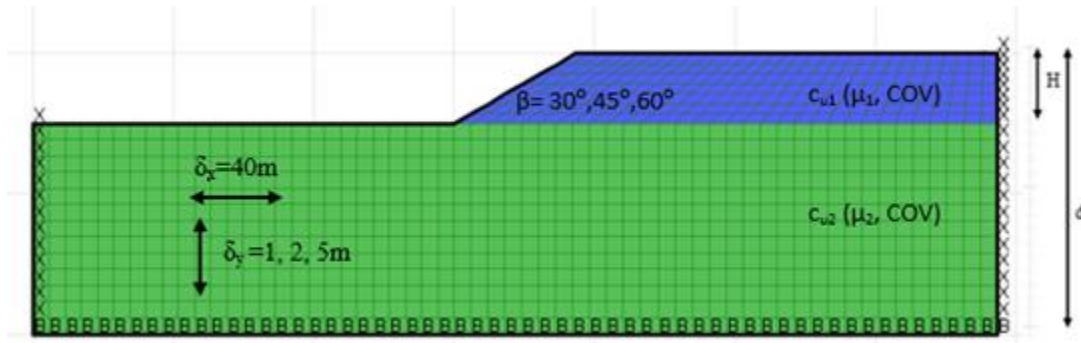


Figure 19. Slope geometry with main input parameters

B. Effect of Random Field of c_{u1} and c_{u2} on Mode of Failure

The mode of failure of the two-layered slope system in the deterministic FLAC analyses conducted in Chapter IV was governed by a deep-seated failure, with the failure surface reaching the rigid boundary (rock layer) under the clay. This mode of failure was dominant, irrespective of the slope geometry or shear strength conditions.

Figure 20 illustrates the model of failure of 8 identical slope cases representing (1) a deterministic failure surface (Fig. 20a) and (b) seven representative Monte Carlo simulations (Fig. 20b-h) from the same random field of c_{u1} and c_{u2} as the deterministic case. The analyzed cases correspond to a typical two-layered slope system with $\beta=45^\circ$, $d/H=3$, $c_{u1}/c_{u2}=5$, $H=5\text{m}$, $\text{COV } c_u=0.5$, $\delta_x=40\text{m}$, and $\delta_y=2\text{m}$. The results on Figure 20 shed light on the importance of modeling the undrained shear strength as a realistic random field which represents the in-situ spatial variability of the soil in the field. A comparison between the failure surface in the deterministic case and the failure surfaces corresponding to the different random realizations for the random field points to significant differences in the shape and location of the failure surface. Unlike the deterministic case where the failure

surface was always deep seated (reaching the rock layer), the failure surfaces in the random simulations showed significant variations in location, shape, and geometry. These results indicate that for any given two-layered slope, the factors of safety from the different realizations could differ from one another leading to a factor of safety (FS) and a stability number (N) that are random variables. The objective of the next section is to quantify the uncertainty in the resulting factor of safety (FS) and stability number (N) by determining their mean, COV, and probability distribution for the different slope cases analyzed.

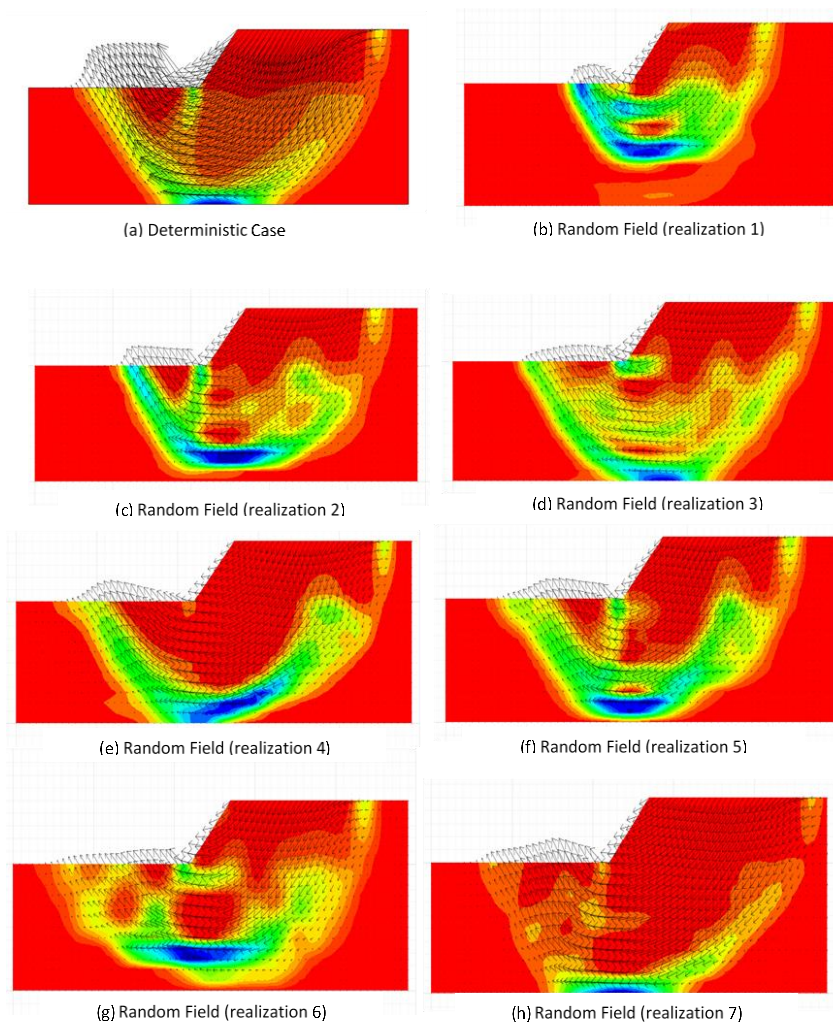


Figure 20. Different failure surfaces for random realizations

C. Analysis of Spatially Random Two-Layered Slopes

To investigate the effect of the spatially random field of S_u on the reliability of the slopes, the same cases that were studied in the deterministic analysis were considered. The base case analysis considers an anisotropic random field with a horizontal correlation length (δ_x) of 40 m and a vertical correlation length (δ_y) of 2m. The horizontal correlation length is kept constant while the vertical correlation length is varied such that (δ_y) is equal to 1, 2, and 5m for each slope angle ($\beta=30^\circ, 45^\circ, \text{ and } 60^\circ$) considered. These assigned values fall in the range suggested by Phoon (1995) who reported horizontal and vertical correlation distances ranging between δ_x of 20m to 70m (mean ~ 45 m) and δ_y of 0.8m to 6.1m (mean ~ 2.5 m). The COV's of the random field of c_{u1} and c_{u2} are taken to be equal for both layers and studied for two COV cases of 0.5 and 0.3. Six values of d/H were selected for the probabilistic analysis ($d/H=1.5, 2, 3, 4, 5, \text{ and } 7$). However, the initial runs indicated similar statistics for the resulting factor of safety for d/H of 4, 5, and 7 (see Fig. 21 for the mean FS). Therefore, $d/H=4$ and 7 were eliminated from the study for the purpose of saving time, and the focus was on the four values of d/H (1.5, 2, 3, and 5).

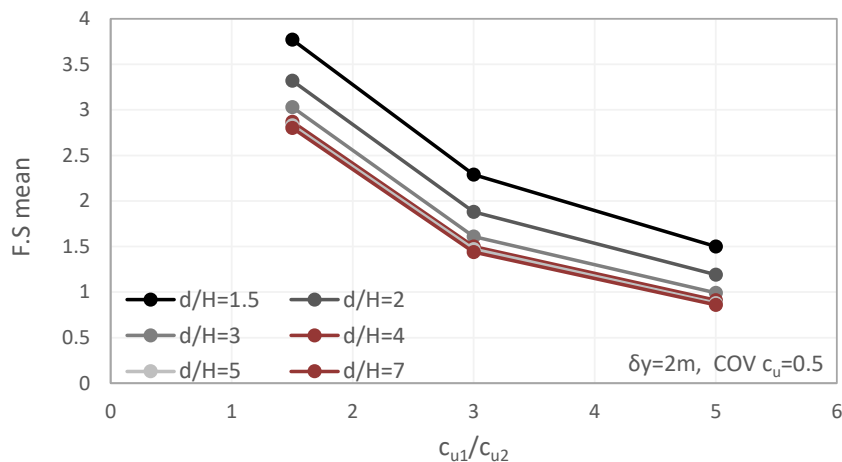


Figure 21. The mean factor of safety with respect to c_{u1}/c_{u2} for different d/H

1. Effect of c_{u1}/c_{u2} , d/H , and COV c_u on Probabilistic Stability Results

In this section, c_{u1}/c_{u2} , d/H , and COV c_u are varied to study their effect on the mean and COV of the factor of safety and the stability number, N . The random field analyses are conducted for the base case with a slope angle $\beta=45^\circ$ and a vertical correlation distance of $\delta_y = 2\text{m}$. The effect of varying the vertical correlation length and the slope angle will be studied and discussed in a later section.

Mean and COV of Factor of Safety

Monte Carlo simulation results were used to calculate the mean and COV of the factor of safety for cases with random fields having COV c_u of 0.3 and 0.5. The variations of the mean and COV of FS with d/H and the mean of c_{u1}/c_{u2} are presented in Fig. 22 and 23, respectively. Results on Fig. 22 indicate that the mean FS decreases as the mean of c_{u1}/c_{u2} increases. For illustration, in the case with a COV c_u of 0.5 and a d/H of 1.5, the mean FS decreases from 3.24 to 1.30 as c_{u1}/c_{u2} increases from 1.5 to 5. Since the mean of c_{u1} was held constant, the decrease in the mean FS is attributed to the weaker undrained strength of the lower layer. The same trend applies to the four d/H cases and the other COV of c_u of 0.3. For a constant mean c_{u1}/c_{u2} , the only governing parameter becomes (d/H) and the mean FS is observed to decrease as d/H increases from 1.5 to 5. Smaller d/H values indicate smaller thicknesses of the weaker layer and thus larger mean FS. In addition, slope systems with smaller “ d ” values are associated with shorter lengths of the failure surface. Shorter surfaces could decrease the effect of variance reduction due to averaging along the failure surface and may lead to smaller mean factors of safety due to higher uncertainty.

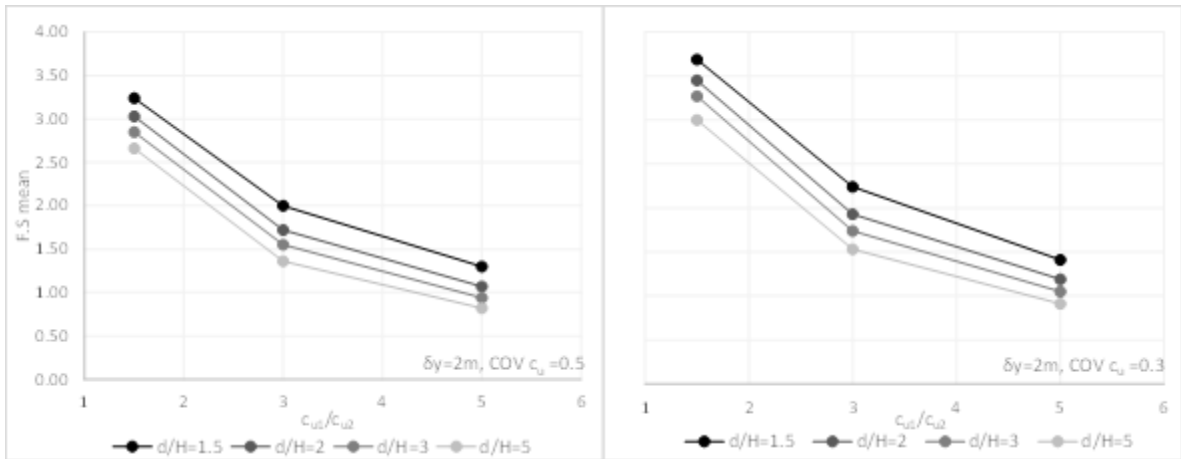


Figure 22. F.S_m with respect to c_{u1}/c_{u2} for different d/H for $COV c_u = 0.5 \& 0.3$

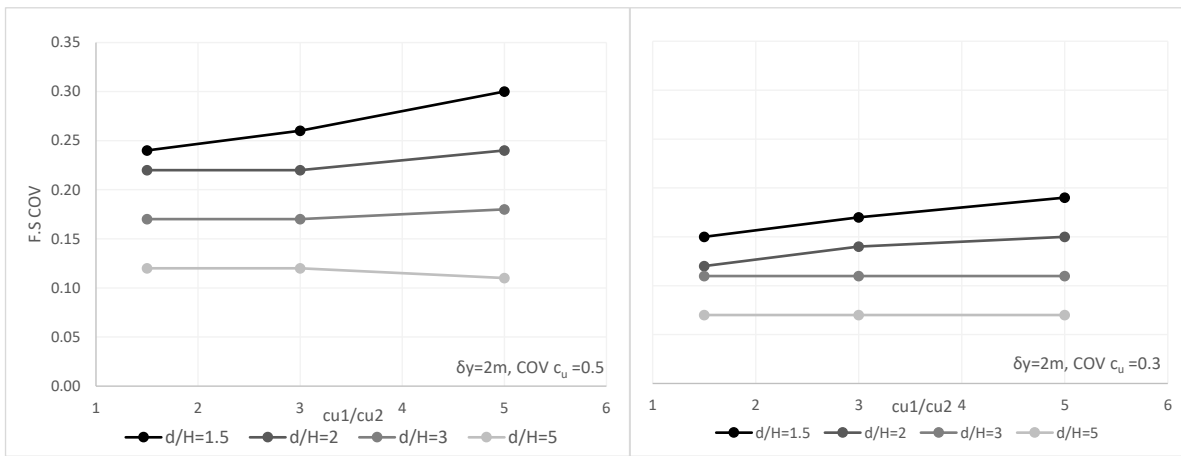


Figure 23. COV of F.S with respect to c_{u1}/c_{u2} for different d/H and for $COV c_u = 0.5 \& 0.3$

The same observations apply to the case with a less uncertain random field of c_u , except that the mean factors of safety were found to be slightly larger in the case involving the lower COV of c_u (compare Fig. 22a to 22b). These results are expected since very low values of c_{u1} or c_{u2} are less likely to be observed in the Monte Carlo simulations for the smaller COV of c_u , leading to mean factors of safety that are larger than those observed for a COV c_u of 0.5, irrespective of the other input parameter. Finally, results on Fig. 22

indicate that the effect of d/H on the mean factor of safety is more pronounced for lower values of mean c_{u1}/c_{u2} .

The effect of the input parameters on the COV of the factor of safety is illustrated in Fig. 23 for the base case analyzed. Unlike the results of the mean factor of safety in Fig. 22, results on Fig. 23 indicate that the COV of FS is more sensitive to the ratio d/H than it is to the ratio of mean c_{u1}/c_{u2} . For illustration, the COV of FS decreases from 0.24 to 0.12 and from 0.3 to 0.11 as d/H increases from 1.5 to 5 for $c_{u1}/c_{u2} = 1.5$ and 5, respectively. The same trends are observed for the cases with $\text{COV } c_u = 0.3$ (Fig. 23b), but with lower COV of FS values. The sensitivity of the COV of FS to the ratio d/H can be directly traced to the phenomenon of variance reduction due to spatial averaging along the length of the failure surface. Large ratios of d/H are associated with longer failure surfaces which allow for more spatial averaging and increased variance reduction leading to a reduced uncertainty in the resulting FS distribution. Lower d/H values are associated with shorter failure surfaces that reduce the impact of variance reduction leading to larger COVs in the resulting FS.

The effect of variance reduction is clearly exhibited in the values of the COV of FS, which are all smaller than the COV of c_u in the random field. For example, the largest COV of FS was about 0.3 for the case involving a COV c_u of 0.5, while the largest COV in FS was about 0.18 for the cases involving a COV c_u of 0.3. Since variance reduction is governed by the ratio of the vertical correlation distance relative to the total length of the failure surface, results in Fig. 23 could only be assumed to be applicable for the case involving a vertical correlation length of 2m. The effect of the correlation length on the probabilistic results is studied in following sections.

Mean and COV of Dimensionless Stability Number (N)

In Chapter IV, the results of the stability analysis of a two-layered clayey slope system were shown to be more conveniently presented using the dimensionless stability number, N . The resulting stability number (N) is not affected by the height of the slope and the actual values of c_{u1} and c_{u2} . Despite the fact that the factor of safety (figures 22 and 23) is more physically meaningful to practicing engineers, it cannot be used to generalize the results of stability analyses done on two-layered systems. As a result, a decision was made to express the deterministic and probabilistic results in this study in the form of the dimensionless stability number (N).

The variation of the mean and COV of N with the input parameters is presented in Fig. 24 and 25, respectively for the base case slope system. The results show that the mean of N (N_m) increases linearly with the ratio of mean c_{u1}/c_{u2} . Since N and FS are inversely proportional, this increase is due to the decrease in the factor of safety which was explained previously. Interestingly, N_m seems to be insensitive to the d/H ratio at small mean c_{u1}/c_{u2} ratios but starts to increase with the d/H ratio at the larger mean c_{u1}/c_{u2} ratios where there is more contrast in the shear strength between the upper and lower clay layers. Differences in the dependence of the mean of FS and the mean of N on d/H and c_{u1}/c_{u2} is related to the fact that the stability number “ N ” includes in its formulation the mean of c_{u1} . When values of “ N ” are calculated in each Monte Carlo simulation, the resulting factor of safety in that simulation is combined with the mean of c_{u1} in that particular simulation and Equation 3.15 is used to calculate “ N ” for that simulation. This normalization of FS by c_{u1} results in differences between the statistics of N compared to the statistics of FS.

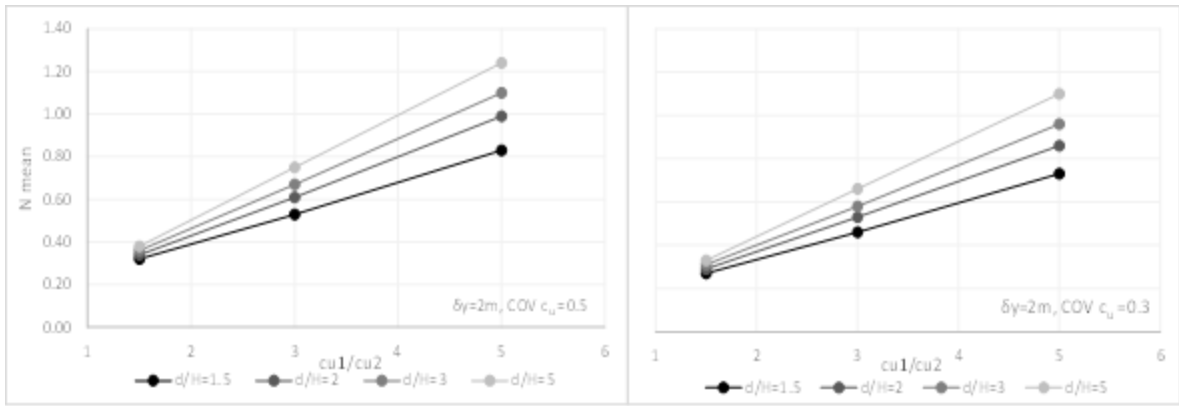


Figure 24. N_m with respect to c_{u1}/c_{u2} for different d/H and for $COV c_u=0.5$ and 0.3

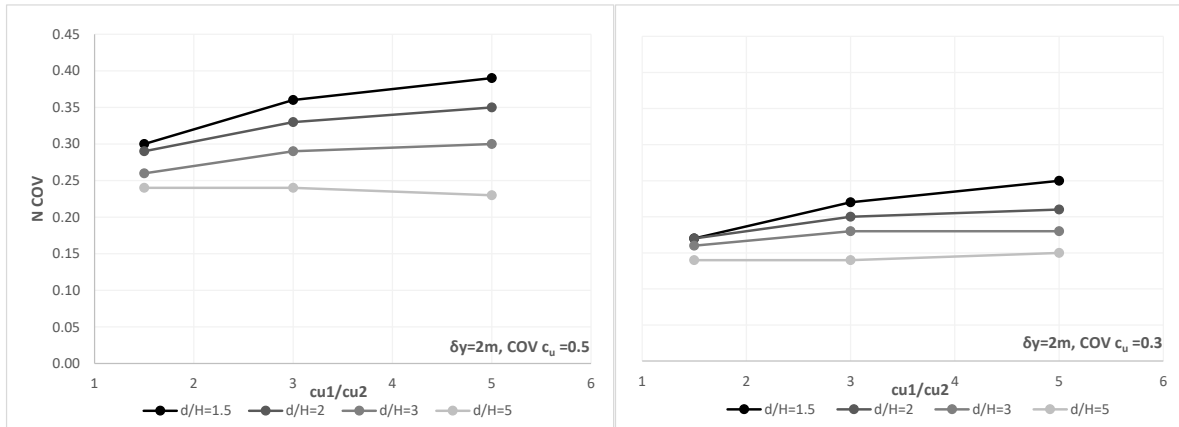


Figure 26. COV of N with respect to c_{u1}/c_{u2} for different d/H and for $COV c_u=0.5$ and 0.3

Regarding the COV of N , results on Fig. 25 indicate that the COV of N is relatively insensitive to c_{u1}/c_{u2} , except for cases involving small d/H ratios where the COV of N is found to increase as c_{u1}/c_{u2} increases. On the other hand, the COV of N clearly decreases as the d/H ratio increases. This is attributed to variance reduction along the longer failure surfaces for the cases involving larger d/H ratios. For illustration, the COV of N is found to decrease from 0.30 to 0.24 and from 0.39 to 0.24 as d/H increases from 1.5 to

5, for cases involving mean c_{u1}/c_{u2} of 1.5 and 5, respectively. The effect of d/H on the COV of N is higher at large mean c_{u1}/c_{u2} ratios

Probability Distribution for the Dimensionless Stability Number (N)

To complete the statistical characterization of the uncertainty in the stability number N , the applicability of a theoretical lognormal distribution in modeling the uncertainty is investigated in this section. Although the exercise was done for multiple slope cases, only results from the case with $d/H=1.5$, $COV_{c_u}=0.5$, $\delta_y=2m$, and $c_{u1}/c_{u2}=5$ will be presented. The statistical test was conducted by comparing the CDF and PDF of the 1500 stability numbers “ N ” which were obtained from FLAC to the PDF and CDF of a typical lognormal distribution with the same mean and standard deviation as the FLAC N -values.

Visual inspection of the comparison between the actual “ N ” distribution and the theoretical lognormal distribution shows an excellent match to the extent that the CDFs of both distributions fully overlap. Q-Q plots for both distributions are also shown on Fig. 27 to further confirm the validity of the lognormal assumption. The results confirm that both sets of data come from the same distribution and as a result the uncertainty in the stability number N for the two-layered slope system can be realistically modeled using a lognormal distribution.

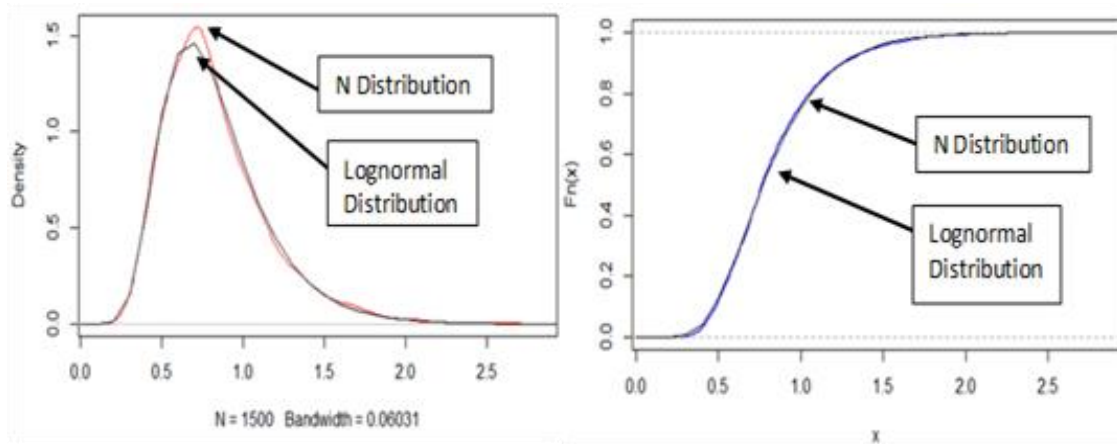


Figure 27. Comparison between the pdf and cdf of N distribution and a lognormal distribution

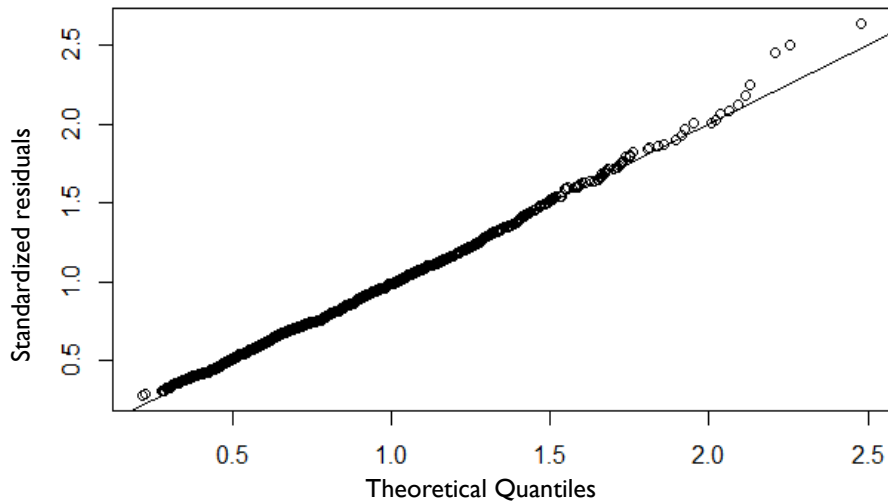


Figure 28. QQ-plot between N distribution and lognormal distribution

2. Effect of the Scale of Fluctuation (SOF) on Statistics of N

The vertical scale of fluctuation (correlation length) is expected to have an impact on the shape and location of the failure surface and on the magnitude of variance reduction due to spatial averaging along the failure surface of the slope system. As a result, the mean and COV of N could be affected by the value of the scale of fluctuation. This Section

investigates the effect of the vertical SOF (δ_y) on the mean and COV of N . This analysis is conducted for the same slope angle ($\beta = 45$) that was used in the previous sections to allow for direct comparison with the previous results. The two additional scale of fluctuations that are assumed are δ_y of 5m and 1m (compared to $\delta_y = 2$ m in the base case).

The effect of the assumed vertical scale of fluctuation on the mean of N is studied on Figs. 28a and 28b for COV c_u of 0.5 and 0.3, respectively. The results show that N_m is not sensitive to the vertical scale of fluctuation. These results are important because they indicate that N_m could be predicted as a function of d/H , mean of c_{u1}/c_{u2} , and the COV of c_u only. This observation will facilitate and simplify the mathematical formulation of models that are needed to predict N_m empirically.

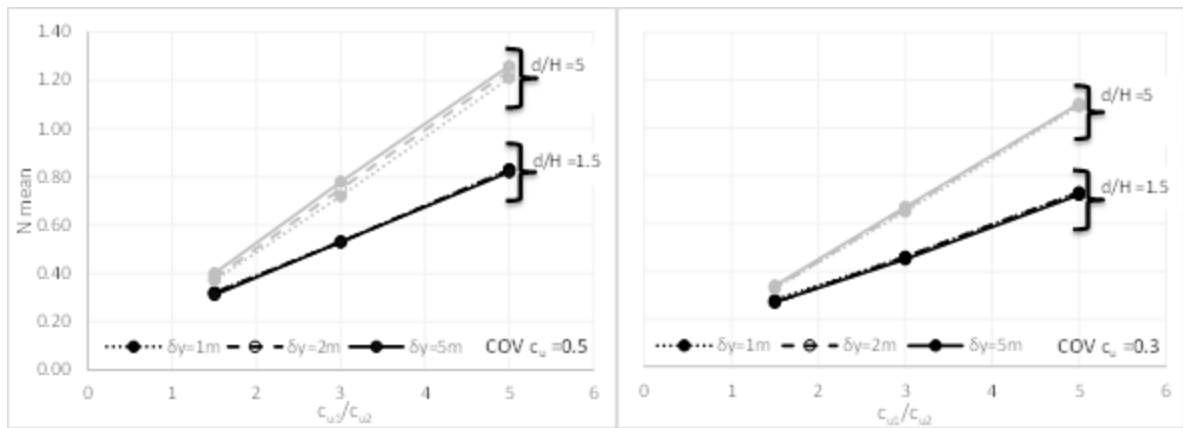


Figure 29. N_m vs. c_{u1}/c_{u2} for COV $c_u=0.5\&0.3$

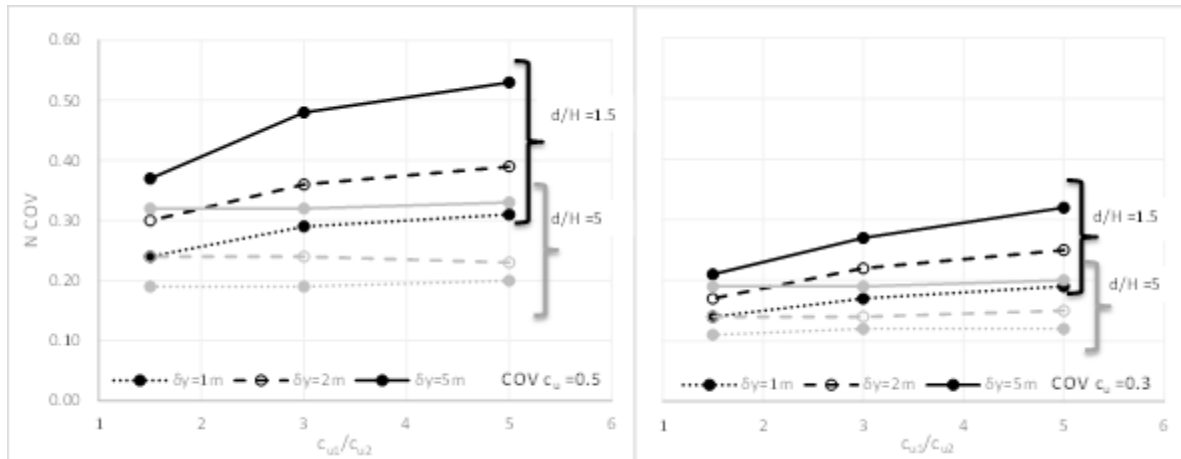


Figure 30. Comparison between COV of N for $\delta y = 1, 2 \& 5m$ for COV $c_u = 0.5 \& 0.3$

Unlike N_m , the COV of N is highly sensitive to the assumed vertical correlation length as indicated in Figure 29. Cases with larger vertical correlation lengths resulted in larger values of the COV of N. This result is expected given that the effect of variance reduction due to averaging decreases dramatically as the correlation lengths approach the length of the failure surface. This explains why cases with d/H values that are small ($d/H = 1.5$) exhibited the least amount of variance reduction resulting in relatively high COV of N. If the results of the COV of N are plotted against the d/H ratio (Fig. 30), a clear decreasing trend in the COV of N is observed with increases in d/H . The sensitivity of the COV of N to the vertical correlation length indicates that the vertical correlation length will play a significant role in determining the reliability of a two-layered slope in clayey soils.

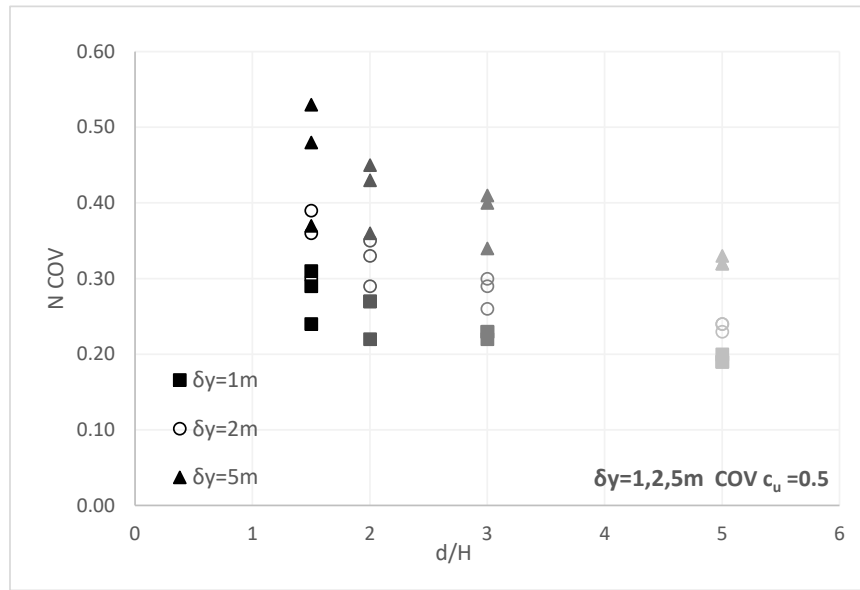


Figure 31. Comparison between COV of N for $\delta y=1, 2\&5m$ for $COV c_u=0.5$

3. Effect of the Slope Inclination Angle (θ) on the Statistics of N

The previous sections studied the effect of four parameters: d/H , c_{u1}/c_{u2} , $COV c_u$ and δy on the probabilistic results of the factor of safety and N distributions. In this section, the focus will be on the effect of the slope angle (β) on the results.

Fig. 31 shows the sensitivity of the mean of N to inclination angle of the slope which was taken to be equal to 30° , 45° , and 60° for cases with $\delta y = 2m$ and $d/H=1.5$ and 3 . As expected, results on Fig. 31 indicate that steeper slopes decrease the factor of safety and increase the mean of the stability number N. The effect of the slope angle on N_m increases for cases with larger mean c_{u1}/c_{u2} ratios and smaller d/H ratios since the role of the upper layer in the stability calculations becomes more significant in these cases.

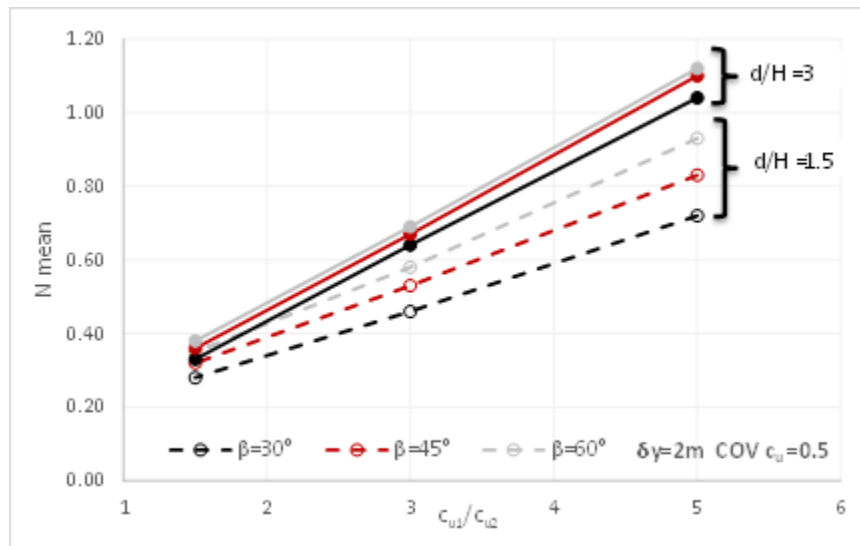


Figure 31. Comparison between Nm for $\beta=30^\circ$, 45° , and 60° for COV $c_u=0.5$

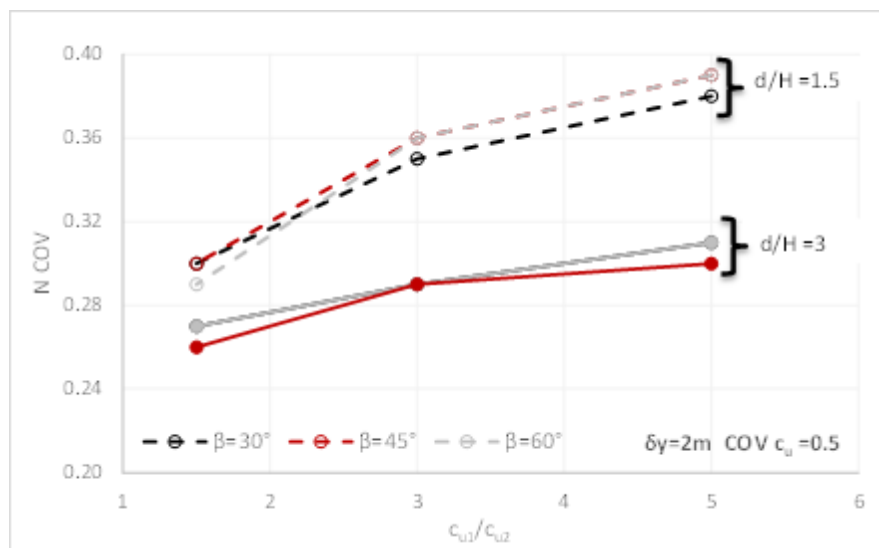


Figure 32. Comparison between COV of N for $\beta=30^\circ$, 45° , and 60°

Fig. 32 shows the effect of $\beta=30^\circ$, 45° and 45° on the COV of N for $\delta_y=2m$ for $d.H=1.5\&3$. The results show almost no effect of β on the COV of N. It can be assumed

that the slope angle has no significant impact on the graphs of COV of N and its effect seems to be the least compared with the four other major parameters studied in this chapter.

CHAPTER VI

RELATIONSHIP BETWEEN DETERMINISTIC AND PROBABILISTIC RESULTS

In Chapter V, the effect of slope geometry, shear strength properties, and random field characteristics on the mean and COV of FS and N was investigated. The main focus for the rest of the thesis will be on linking the deterministic stability factor (N) obtained using FLAC or through the simplified empirical model presented in Equation 3.16 to the probabilistic output relating to the mean and COV of the stability number N. The aim is to reach a stage where the statistical parameters of N can be predicted from the deterministic results without the need to go through the tedious simulations in FLAC. The relationship between the deterministic and probabilistic results will be established by studying the dependency of the ratios N_m/N_d and $COV(N)/COV(c_u)$ on the input parameters affecting the stability of two-layered clayey slope systems. These parameters include: c_{u1}/c_{u2} , δ_y , d/H , $COV c_u$, and β .

A. Relationship between N_m/N_d and $COV c_u$

The variation of the ratio N_m/N_d with the COV of c_u is presented in Fig. 33 for the three slope angles considered in this study. Some additional runs were made for a random field with a COV of c_u of 0.1 to establish the complete trend. Results on Fig. 33 clearly show that the ratio of N_m/N_d increases from values of unity for the case with the least uncertain random field of c_u ($COV = 0.1$) to values in the range of 1.17 to 1.40 for the cases involving the most uncertain random field ($COV = 0.5$). The observation that the mean value of N is larger than the deterministic value of N for larger COVs is realistic and

is related to the fact that the mean of FS becomes smaller than the deterministic value of FS for large COVs of c_u . This trend is similar for the three slope angles.

It is worth noting that the lower boundaries for all COV's are associated with $\delta_y = 5\text{m}$, $d/H=1.5$, $c_{u1}/c_{u2}=1.5$ and the upper boundaries belong to $\delta_y = 5\text{m}$, $d/H=5$, $c_{u1}/c_{u2}= 1.5$. The extreme values belong to the highest SOF, the lowest and highest d/H respectively, and the lowest c_{u1}/c_{u2} ratios. This can be explained by the fact that high SOF's decrease spatial averaging which increases the difference between N_m and N_d . The fact that d/H governs the upper and lower bounds of the variation of N_m/N_d is expected given the strong impact that d/H had on the resulting N_m values as indicated in Figure 24. It is worth noting that although not all the cases for $\beta=60^\circ$ were simulated it can be concluded from Figure 33 that (N_m/N_d) generally increases as β increases.

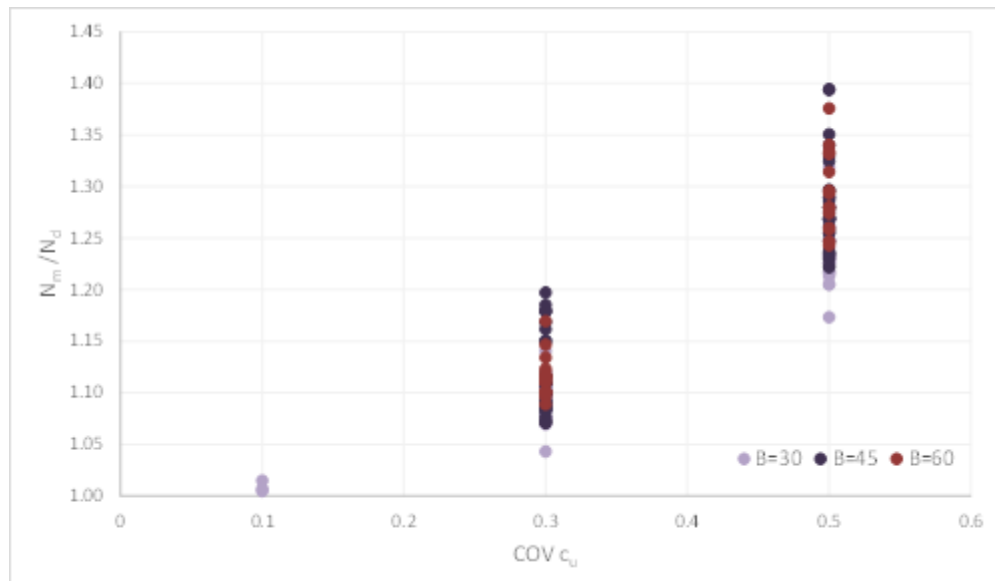


Figure 33. N_m/N_d with respect to $COV c_u$ for $\beta=30^\circ$, $\beta=45^\circ$, and $\beta=60^\circ$

B. Relationship between N_m/N_d and c_{u1}/c_{u2}

The variation of N_m/N_d with c_{u1}/c_{u2} is plotted on Fig. 34 for the three δ_y 's and for a slope angle of 30° and for the two COV's of c_u (0.5 and 0.3) considered. The results of Fig. 35 show two sets of graphs, the upper set of solid lines belongs to COV $c_u=0.5$, and the lower set of dashed lines belongs to COV $c_u=0.3$. These results indicate that the COV of c_u plays a much more significant role in determining the ratio N_m/N_d compared to the ratio c_{u1}/c_{u2} which does not seem to have a strong impact on the results. An average line crossing the lower bundle of curves results in (N_m/N_d) of 1.1 with some scatter above and below as high as 1.14 and as low as 1.04 for c_{u1}/c_{u2} less than 3. d/H values of 3 and 5 set the limit for the upper bound and d/H values of 1.5 and 2 set the limit for the lower. The average of the upper bundle of graphs (COV $c_u = 0.5$) has an average (N_m/N_d) of 1.25 with higher scatter around the average compared to the results of COV $c_u=0.3$.

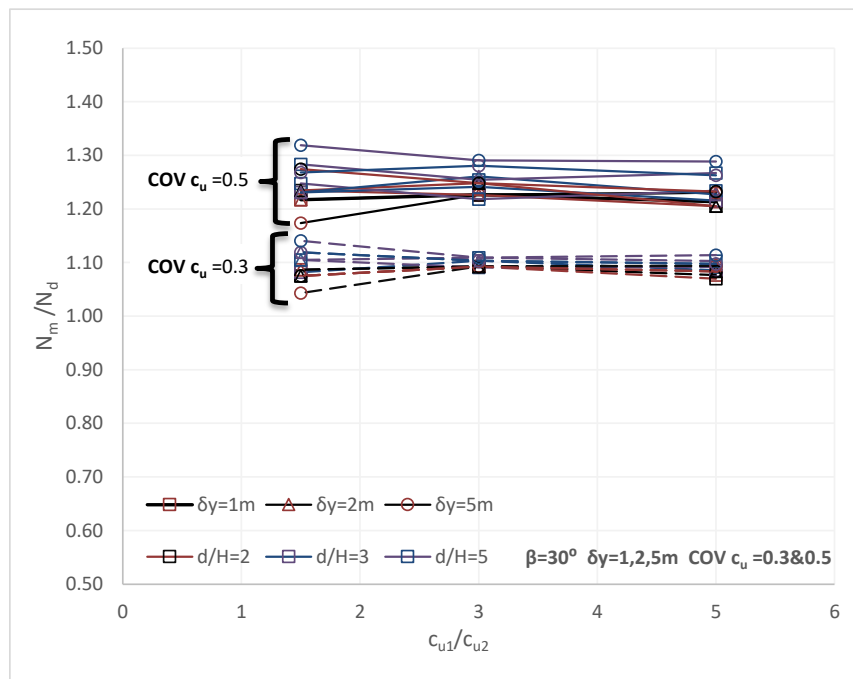


Figure 34. N_m/N_d with respect to c_{u1}/c_{u2} for $\beta=30^\circ$

In summary, the results of Figs. 33 and 34 show a clear effect of the slope angle, COV of the undrained shear strength, the scale of fluctuation, and the d/H ratio on the ratio N_m/N_d . The least significant impact is for the undrained shear strength ratio.

C. Relationship between COV N/COV c_u and c_{u1}/c_{u2}

In this section, the relationship between (COV N/COV c_u) and the major factors will be investigated in an attempt to establish simple equations that would allow for predicting COV N/COV c_u without the need for expensive random fields using FLAC.

The variation of COV N/COV c_u with (c_{u1}/c_{u2}) is presented on Fig. 35 for the two extreme d/H conditions (1.5 and 5.0) and the three vertical correlation lengths (δ_y of 1m, 2m, and 5m) considered in this study. The analysis is presented for the case with a slope angle $\beta=30^\circ$ for illustration. The major finding in Fig. 35 is that the ratio COV N/COV c_u seems to be largely insensitive to the level of uncertainty in the random field of c_u . This is shown on Fig. 35 by comparing the dotted (COV $c_u = 0.3$) and solid (COV $c_u = 0.5$) lines for any given combination of d/H and δ_y . This observation is of extreme importance since it points to the strong role that that the COV N/COV c_u ratio could play in linking the probabilistic results to the deterministic results and the input parameters.

The other conclusion from Fig. 35 is that the ratio COV N/COV c_u is highly sensitive to the d/H ratio and the vertical scale of fluctuation δ_y . This is expected given the trends that were observed for the COV N with d/H and δ_y in Fig 30. The d/H ratio is directly correlated to the length of the failure surface, so both d/H and δ_y govern the degree of variance reduction due to spatial averaging which will eventually dictate the resulting COV N. The results also

show that the ratio c_{u1}/c_{u2} plays a role in defining the $COV N_m/COV c_u$ particularly for small d/H values where the ratio of $COV N_m/COV c_u$ is observed to increase as the contrast between the strength of the upper and lower layer increases. This result can be explained by the fact that for cases with small d/H ratios where the softer layer is relatively thin, the failure surface in the lower (softer) layer is generally horizontal. Variance reduction along flat horizontal portions of the failure surface is expected to be minimal given that the undrained strength was assumed to have a relatively long correlation distance in the horizontal direction ($\delta_x = 40m$). This condition is amplified for cases with large c_{u1}/c_{u2} values of 5.0 since the factor of safety and thus the stability number N in these cases are governed by the lower soft clay layer. Given that variance reduction in this layer will be minimal as discussed, this will lead to minimal variance reduction in the case of small d/H ratios and large c_{u1}/c_{u2} as indicated in Figure. 35.

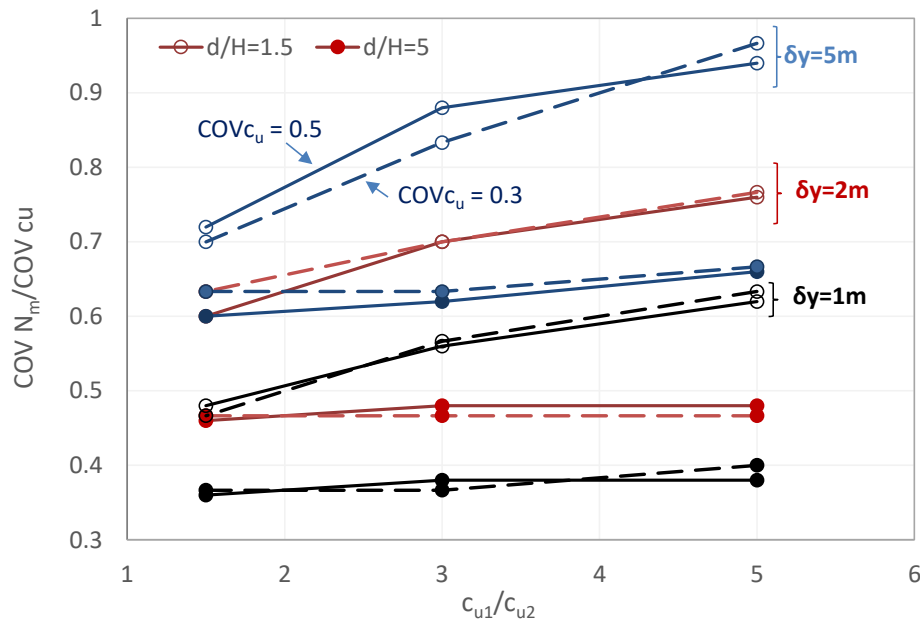


Figure 35. Dependence of $COV N_m/COV c_u$ on Input Parameters ($\beta = 30^\circ$)

D. Relationship between COV N/COV c_u and $\delta_y/L.FS$

The results in section C show that the ratio COV N / COV c_u is mostly governed by variance reduction due to averaging along the failure surface. The main parameter that governs variance reduction is the ratio $\delta_y / L.FS$ where L.FS is defined as the length of the failure surface and could be estimated from the results of the deterministic analysis conducted in FLAC for any set of input parameters. The ratio $\delta_y / L.FS$ embeds in it the effects of the vertical scale of fluctuation and the d/H ratio which have been shown to have a direct impact on the COV N / COV c_u ratio. In addition, this ratio will indirectly reflect changes in the angle of the slope β since the length of the failure surface will be affected by the choice of β . The only parameter that is not captured in the ratio $\delta_y / L.FS$ is c_{u1}/c_{u2} ratio.

The $\delta_y/L.FS$ ratio was calculated for all the cases analyzed in this study and plotted versus the COV N / COV c_u on Figure 36. The results in Fig. 39 show that as $\delta_y / L.FS$ increases, the COV of N/COV c_u increases till it reaches a horizontal asymptote at ($\delta_y / L.FS=0.2$), whereby any increase in $\delta_y / L.FS$ results in negligible effect on the COV N/COV c_u . This trend is observed in the three different slope angles with a minor deviation to the right as β increases, which shows little effect for the slope angle on the results as expected. The increase in the ratio of COV N/COV c_u towards a ratio of 1 implies an increase in the COV of N to reach the input COV of the undrained shear strength distribution. This behavior is logical and can be attributed to the dual effect of δ_y and d/H which are both reflected in $\delta_y / L.FS$. Increases in $\delta_y / L.FS$ imply either a large correlation length or a short failure surface, both which result in less variance reduction due to averaging, dictating the value of the COV of N.

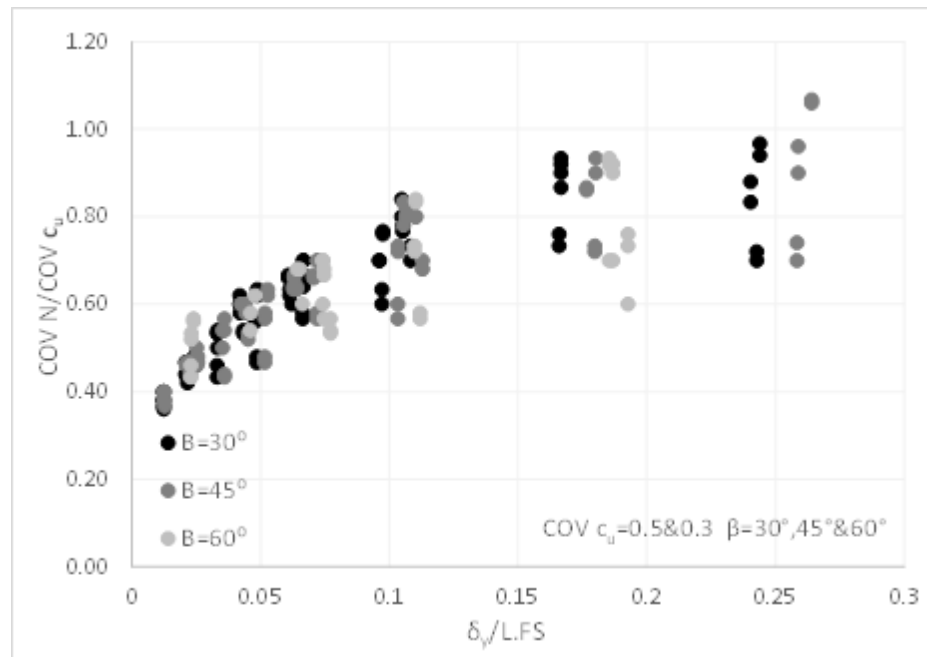


Figure 36. $\text{COV } N / \text{COV } c_u$ with respect to $\delta_y / L.FS$

The scatter in trend shown in Fig. 36 is explained by the fact that the COV of N is also affected by the relative strength between the first and the second layer. This is reflected in the ratio c_{u1}/c_{u2} which is not taken into consideration in the relationship shown in Fig. 36. The impact of the c_{u1}/c_{u2} on the ratio $\text{COV } N / \text{COV } c_u$ should be included in any empirical relationship that could be established to more reliable predictions of the ratio of $\text{COV } N / \text{COV } c_u$ for two-layered slope systems with stiff clays resting on softer clays. However, the relationship in Fig. 36 could serve as a first order approximation for predicting $\text{COV } N / \text{COV } c_u$ as a function of $\delta_y / L.FS$ only.

CHAPTER VII

RELIABILITY DESIGN OF SPATIALLY VARIABLE MULTI-LAYERED CLAYEY SLOPES

In this chapter, simplified empirical correlations that link the ratios N_m/N_d and the COV $N/COV c_u$ to the main input parameters that were shown to affect the statistics of N are presented. The analysis is based on the results presented in Chapter VI.

A. Mean of N as a function of COV c_u

The dependency between the ratio N_m/N_d and the COV of c_u was thoroughly investigated in Chapter VI and it was shown that the mean of N was proportional to the COV of c_u as indicated in Fig. 37. Using regression, a simple second order polynomial was used to fit the data. The resulting relationship is presented in Equation 7.1 and consists of a second order polynomial.

$$\frac{N_m}{N_d} = 0.7475COV^2 + 0.1799COV + 0.9829 \quad (\text{Eq. 7.1})$$

The empirical equation produces reasonable estimates of N_m/N_d with an R^2 value of 0.91. To quantify the predictive performance of the simple relationship in Eq. 7.1, twenty five additional independent slope cases involving different combinations of the input parameters and random fields of c_u (see Appendix 2) were analyzed in FLAC. The resulting FLAC-predicted N_m/N_d were calculated and compared to the N_m/N_d ratios that were predicted using the simple quadratic correlation of Equation 7.1 on Figure 38. The results indicate an acceptable level of predictive performance with no apparent bias in the

model predictions and relatively low uncertainty around the mean trend. To quantify the model uncertainty, the ratio of FLAC (N_m/N_d) to predicted (N_m/N_d) was calculated for the 60 cases analyzed. The mean of this ratio was calculated to be 0.98 while the COV of this ratio was around 0.02. These statistics indicate that Equation 7.1 is a cheap alternative for determining a first order estimate of the ratio N_m/N_d for two layered slope systems.

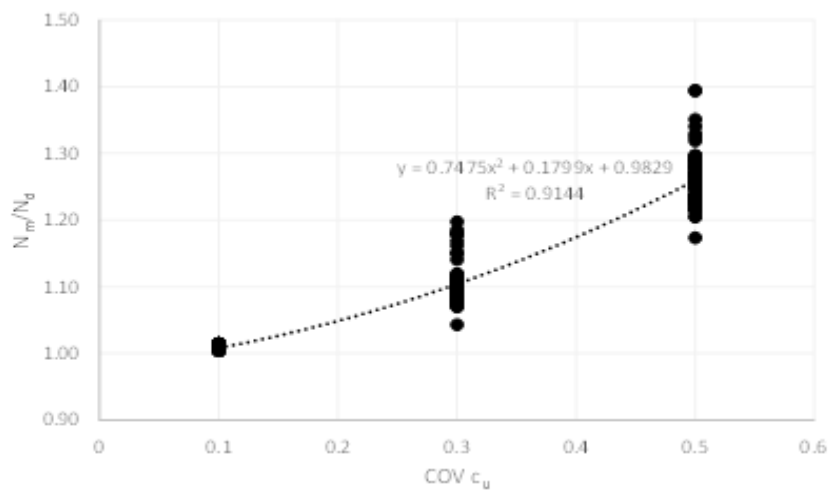


Figure 37. Model for N_m/N_d vs. $COV c_u$

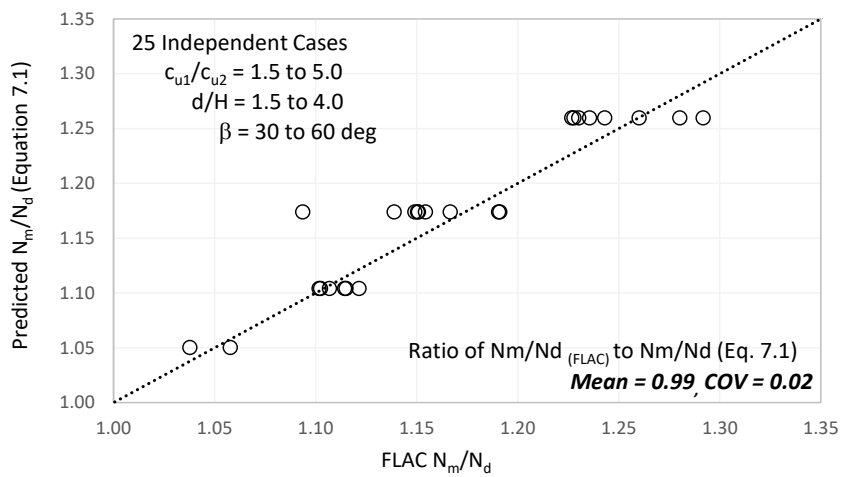


Figure 38. Effectiveness of Model Predictions of Equation 7.1

B. (COV N/COV c_u) as a function of (δ_y /length of the failure surface)

The analysis pertaining to the ratio COV N / COV c_u indicated a strong dependency on the ratio δ_y /L.FS as illustrated in Fig. 39. This dependency could be modeled using a logarithmic function as per Equation 7.2 such that:

$$\frac{COV N}{COV c_u} = 0.1765 \ln\left(\frac{\delta_y}{L.FS}\right) + 1.1248 \quad (\text{Eq. 7.2})$$

The empirical equation produces reasonable estimates of COV N / COV c_u with an R^2 value of 0.84. To quantify the predictive performance of the simple relationship in Eq. 7.2, the twenty five additional independent slope cases were used as indicated in Figure 40. The results indicate that although the equation produces estimates of (COV N / COV c_u) that are relatively unbiased, the predictions scatter significantly around the equality line with a relatively large estimated coefficient of variation 0.1.

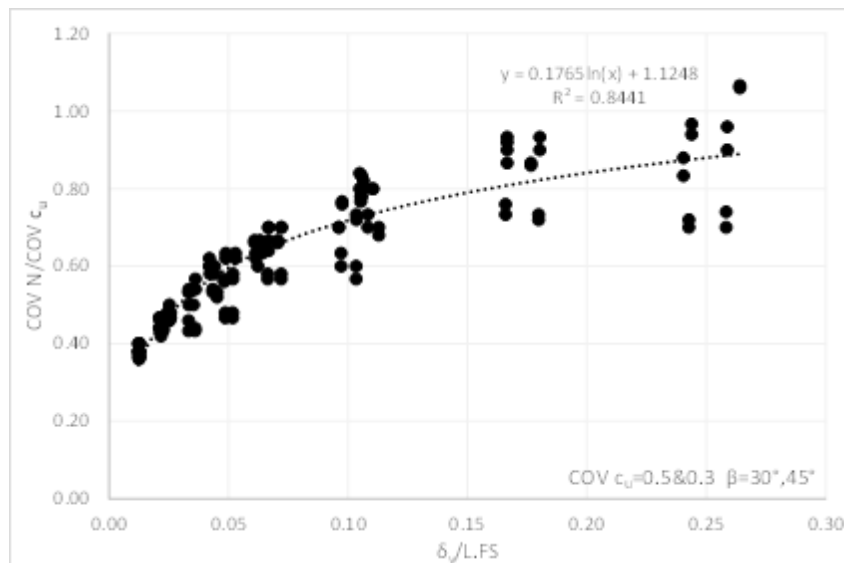


Figure 39. COV N/COV c_u with respect to δ_y /L. FS for COV $c_u=0.5\&0.3$

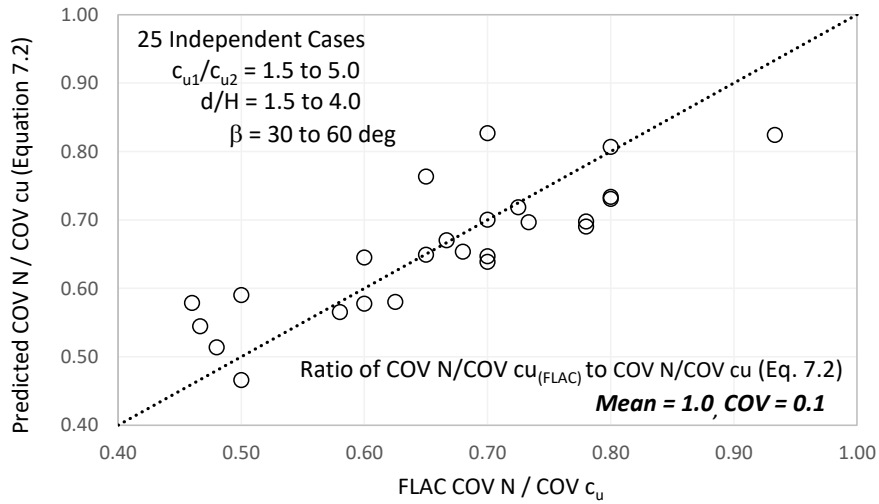


Figure 40. Effectiveness of Equation 7.2 in predicting the ratio of COV N/COV c_u

C. Regression Models for Predicting Mean and COV of N in Multi-Layered Slopes

1. Regression Model for (N_m/N_d)

In analyzing the results of chapters V and VI, it was shown that the statistical parameters (mean and COV) of N are influenced by four main factors: (1) the coefficient of variation of the undrained shear strength (COV c_u), (2) the undrained shear strength of the first layer divided by the undrained shear strength of the second layer (c_{u1}/c_{u2}), (3) the d/H ratio, (4) the angle of the slope β which will be included as $\tan\beta$, and (5) the scale of fluctuation δ_y . A decision was made to normalize the vertical scale of fluctuation by the total vertical height of the combined slope system (d) and to include the normalized parameter δ_y/d in the regression model.

Using solver add-in in excel worksheet, the objective was to minimize the error between the predicted results using the empirical model and the measured results in FLAC

by changing the values of each parameter. The general mathematical form of the empirical model that was calibrated using regression is presented in Equation 7.3. The model calibration exercise was conducted using the excel solver to calculate the 6 parameters involved (a, b, c, d, e, and f):

$$\frac{N_m}{N_d} = f \cdot \left(\frac{\delta y}{d}\right)^a \cdot \left(\frac{c_{u1}}{c_{u2}}\right)^b \cdot (COV)^c \cdot (\tan \beta)^d \cdot \left(\frac{d}{H}\right)^e \quad (\text{Eq.7.3})$$

Where N_m represents the mean of the probabilistic dimensionless number N , and N_d represents the deterministic value of N . Minimizing the summation of square error to a value of 0.09, the values of a, b, c, d, e, and f were found to be equal to 0.009, -0.012, 0.265, 0.034, 0.049, and 1.5 respectively. The empirical equation to calculate N_m/N_d is now shown in Eq. 7.4 as:

$$\frac{N_m}{N_d} = 1.5 \left(\frac{\delta y}{d}\right)^{0.009} \cdot \left(\frac{c_{u1}}{c_{u2}}\right)^{-0.012} \cdot (COV)^{0.265} \cdot (\tan \beta)^{0.034} \cdot \left(\frac{d}{H}\right)^{0.049} \quad (\text{Eq.7.4})$$

The bias and uncertainty of the above regression model was investigated on Figure 41 which compares measured and predicted N_m/N_d values. Results indicate that the ratio of FLAC (N_m/N_d) to the predicted (N_m/N_d) has a mean of 0.99 with a COV of 0.03. A closer look at the model predictions indicate that the model slightly under predicts N_m/N_d for small values of N_m/N_d (generally associated with small values of COV of c_u) and very slightly over predicts N_m/N_d for larger N_m/N_d values. The model however provides satisfactory predictions that allow the user to predict the mean value of N as a function of the deterministic N value and all the other parameters presented in Equation 7.4.

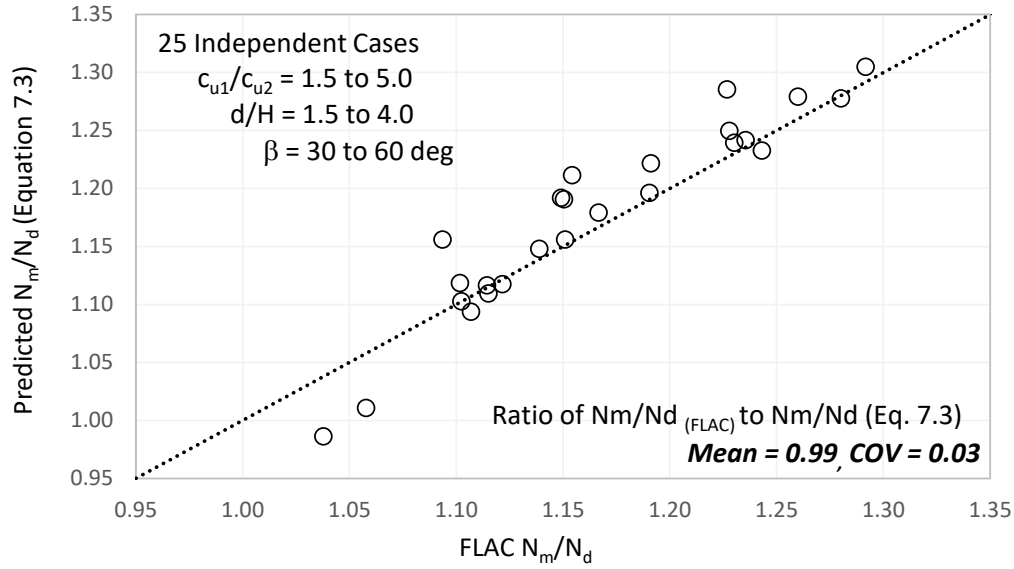


Figure 41. Effectiveness of Equation 7.4 in predicting the ratio of N_m/N_d

2. Regression Model for $(COV N / COV c_u)$

Following the same procedure, an empirical model that predicts the ratio $COV N / COV c_u$ as a function of the main parameters that were found to affect the problem was calibrated using regression resulting in:

$$\frac{COV N}{COV c_u} = 1.117 \cdot \left(\frac{\delta y}{L.FS}\right)^{0.279} \cdot \left(\frac{c_{u1}}{c_{u2}}\right)^{0.168} \cdot (COV)^{0.004} \cdot (\tan \beta)^{-0.014} \quad (\text{Eq.7.5})$$

To quantify the predictive performance of the model, the twenty five additional independent slope cases were used. The results are presented on Fig. 42 and indicate the model produces estimates of $COV N / COV c_u$ that are relatively unbiased and that the predictions scatter in the model predictions about the line of equality was reduced compared to the simplified model in Equation 7.2 whereby $COV N / COV c_u$ was expressed solely as a function of $\delta y/L.FS$. This reduction in the model uncertainty is reflected in the

smaller COV value of 0.07 for the regression model of Equation 7.5 (compared to a COV of 0.10 for the simplified empirical model of Equation 7.2).

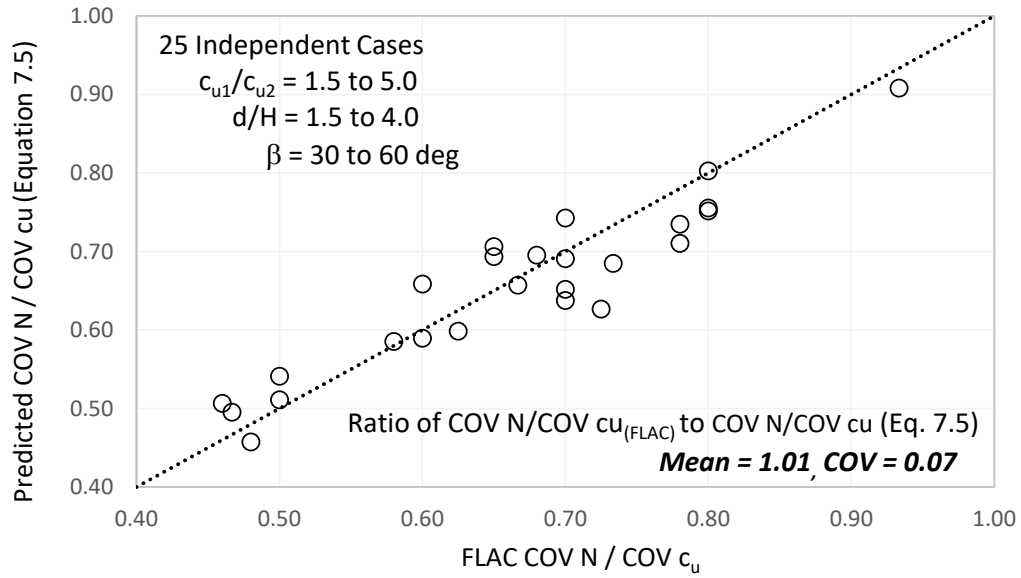


Figure 42. Effectiveness of Equation 7.5 in predicting the ratio of COV N/COV c_u

CHAPTER VIII

DESIGN EXAMPLE

In this chapter, a design example for a two-layered slope system is presented to illustrate the methodology in which the results of this research study could be used in practical design scenarios. The main objective is to link the deterministic design factor of safety of a two-layered slope system to the probability of failure of the slope without the need to conduct expensive FLAC models with random fields.

The example involves investigating the reliability of a two layered slope system that is designed using different deterministic factors of safety. For illustration, the slope will be assumed to have a fixed slope angle $\beta = 50$ degrees. The height of the slope in the first layer is assumed to be a design parameter that varies with the design factor of safety while the thickness of the second layer is assumed to be fixed at 15m (see Fig. 43). The unit weight of both clay layers is assumed to be equal to 20 KN/m^3 while the random fields of the undrained shear strength in the two clay layers are described by $\mu_{c_{u1}}=100 \text{ kpa}$, $\text{COV}_{c_u}=0.3$, $c_{u1}/c_{u2}=4$, and $\delta y=3\text{m}$.

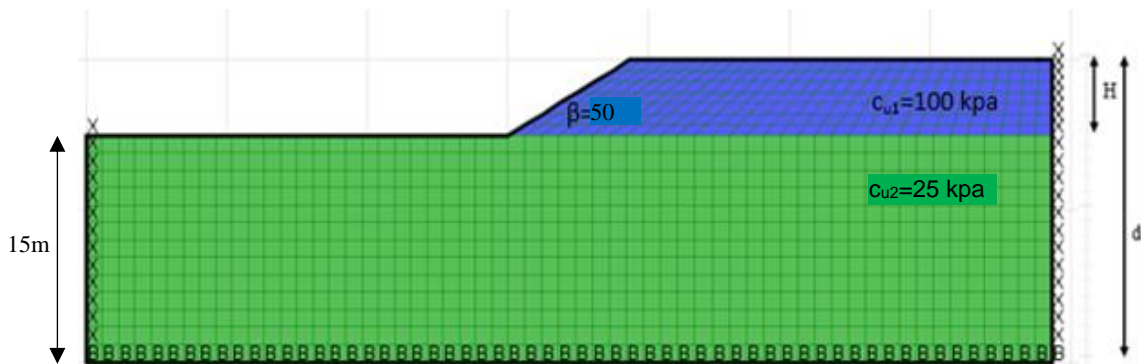


Figure 43. Geometry and Soil Properties of the illustrative Design Example

The initial analysis involves finding the probability of failure of the slope system for a typical deterministic design factor of safety of 1.5. The probability of failure could be quantified following the step by step procedure outlined below:

- The first step involves calculating the height of the slope that would result in a deterministic factor of safety of 1.5. This normally requires modeling the two layered system on FLAC. Alternatively, the simplified empirical model in Equation 3.16 for N_d could be used to calculate H such that:

$$\frac{c_{u1}}{\gamma * H * F.S} = 0.141 \cdot \left(\frac{c_{u1}}{c_{u2}}\right)^{0.942} \cdot (\tan \beta)^{0.092} \cdot \left(\frac{d}{H}\right)^{0.245}$$

Which gives **H=4.38m** making the total height of the slope system equal to **d=19.38m**.

- The second step is to calculate the deterministic value of N_d that corresponds to the deterministic factor of safety (FS = 1.5):

$$N_d = \frac{100}{20 * 4.38 * 1.5}$$

Which gives **$N_d=0.76$** .

- The third step is to calculate the mean value of N_m using Eq. 7.1:

$$\frac{N_m}{N_d} = 1.532 \cdot \left(\frac{3}{19.38}\right)^{0.009} \cdot (4)^{-0.012} \cdot (0.3)^{0.265} \cdot (\tan 50)^{0.034} \cdot \left(\frac{19.38}{4.38}\right)^{0.049}$$

Which gives **$N_m=0.8$** .

- The fourth step is to calculate the COV of N using Eq. 7.5:

$$\frac{COV N}{COV c_u} = 1.117 \cdot \left(\frac{3}{L.FS}\right)^{0.279} \cdot (4)^{0.168} \cdot (0.3)^{0.004} \cdot (\tan 50)^{-0.014}$$

Which gives **COV N=0.18**.

- The fifth step is to check the probability of failure, which is calculated as:

$$Pf = p(F.S < 1) = P(N > 1.142) = 1 - P(N < 1.142) = 1 - \Phi\left(\frac{\ln(1.142) - \lambda}{\vartheta}\right)$$

$$\text{Where } \lambda = \ln Nm - \frac{\vartheta^2}{2} \text{ and } \vartheta = \sqrt{\ln(1 + COV^2)}$$

➡ Which gives **pf=3.9%**.

The above procedure could be repeated for other deterministic factors of safety and different random fields of c_u . For illustration, the above calculation is repeated for four COV c_u values of 0.2, 0.3, 0.4, and 0.5 and for seven design factors of safety (F.S=1.3, 1.4, 1.5, 1.6, 1.7, 1.8, 1.9, 2.0). The resulting probabilities of failure are presented in Fig. 44 as a function of the design F.S for each COV c_u . As expected, results of the reliability analysis indicate that the probability of failure decreases as the factor of safety increases and as the COV of c_u increases.

The results on Figure 44 were obtained without the need for running any probabilistic analysis in FLAC. These results could be used to select the design factor of safety (and thus the design height of the slope) that would ensure a target level of risk in the two-layered slope system. The results of such an analysis are presented in Fig. 45. The results on Fig.

45 indicate that the design height of the slope depends on the target probability of failure and on the assumed COV of c_u . As a example, for the case with a COV c_u of 0.3, the height of the slope will have to be reduced from 4.5m to 3.9m if the target probability of failure is decreased from 5% to 1%.

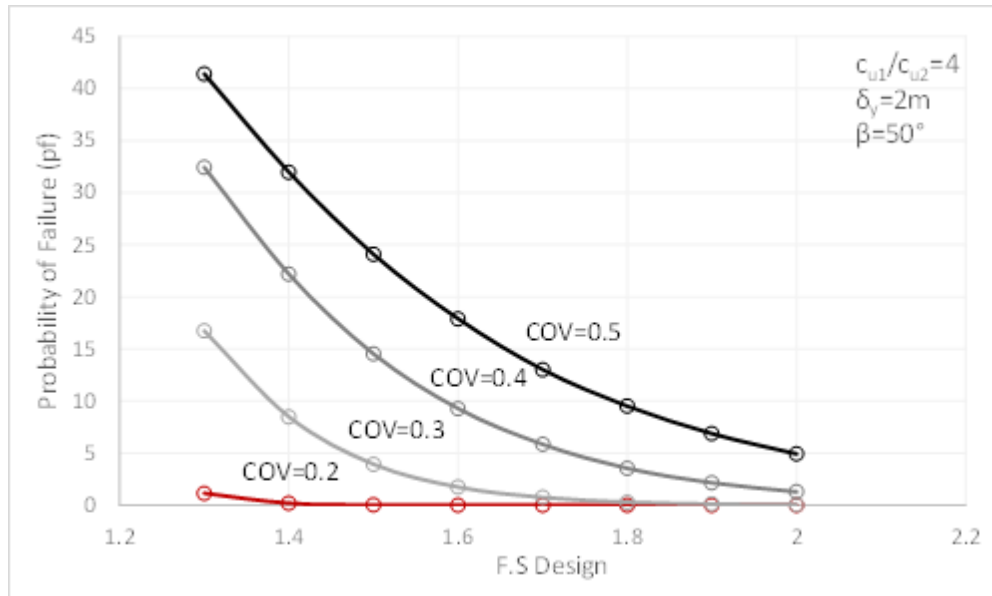


Figure 44. Probability of failure (pf) vs. FS design

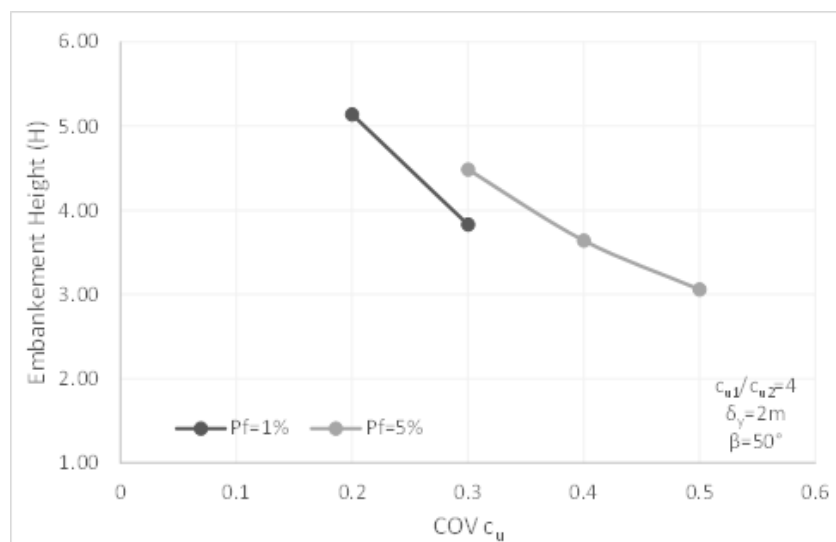


Figure 45. Embankment Height (H) vs. COV c_u

CHAPTER IX

CONCLUSIONS

In this thesis, the reliability of spatially variable two-layered slopes was studied and analyzed using FLAC software. The importance of this work comes from the need to consider the effect of spatial variability of soil on the resulting risk of failure of two-layered slopes. The effect of different slope geometries (slope height and angle), soil parameters, and random field properties was taken into account to draw relationships between the deterministic and the probabilistic results. The main focus in establishing these relationships was on the statistics of the dimensionless stability number N . The established relationships allow designers to predict the probability of failure in a simplified manner without the need for complicated and computationally expensive numerical analyses using random fields.

The main parameters that were varied include the ratio of the slope height to the total height of the slope system (d/H) ranging from 1.5 to 5, the ratio of the upper mean undrained shear strength to the lower mean undrained shear strength ranging from 1.5 to 5, the slope angle ranging from 30° to 60° , the coefficient of variation of the undrained shear strength of 0.3 and 0.5, and the vertical correlation length ranging from 1 to 5m. The anisotropy in the random field is reflected in the horizontal correlation length which was kept constant throughout the study with a value of 40m.

Upon the generation of random fields using R software and mapping them to their respective elements through FISH functions, FLAC was utilized to calculate the statistical

parameters of the stability number N . It should be noted that the undrained shear strength is the only source of uncertainty that was incorporated in the analysis. Based on the results of the analyses conducted in this study, the following conclusions can be made:

1. A simplified empirical equation that allows the designer to predict the deterministic dimensionless stability number N_d without the need for running computationally demanding numerical analyses using FLAC was developed based on the results of FLAC. The empirical equation expresses N_d as a non-linear function of β , d/H , and c_{u1}/c_{u2} (Eq. 3.16). The mathematical formulation of the established model is simple and points to the significant impact of c_{u1}/c_{u2} and the negligible impact of the slope angle β on the results.
2. An investigation of the mode of failure of two-layered slope systems pointed to the importance of modeling the undrained shear strength as a realistic random field which represents the in-situ spatial variability of the soil. A comparison between the failure surface in the deterministic case and the failure surfaces corresponding to random fields shows significant differences in the shape and location of the failure surface. Unlike the deterministic case where the failure surface was always deep seated (reaching the rock layer), the failure surfaces in the random simulations showed significant variations in location, shape, and geometry.

3. An investigation of the relationship between the mean value of N (N_m) and the deterministic N (N_d) showed that strong positive correlation exists between the ratio N_m/N_d and the COV of c_u . A simple quadratic relationship was established between N_m/N_d and the COV of c_u to provide first order approximations of this ratio. A more comprehensive empirical model that expresses N_m/N_d as a function of (1) the COV c_u , (2) the ratio of mean (c_{u1}/c_{u2}), (3) the d/H ratio, (4) the angle of the slope β and (5) the scale of fluctuation δ_y was also calibrated using the FLAC results to provide more reliable predictions of N_m/N_d .
4. With regards to the uncertainty in the stability number N , it was concluded that the ratio $\text{COV } N / \text{COV } c_u$ is a convenient parameter for generalizing the probabilistic results for two-layered soil systems. The ratio $\text{COV } N / \text{COV } c_u$ exhibited a strong dependency on the ratio $\delta_y / L.FS$, where δ_y is the vertical correlation length and $L.FS$ is the length of the failure surface. This dependency was modeled using a logarithmic function which was shown to produce reasonable estimates of $\text{COV } N / \text{COV } c_u$ that are relatively unbiased and characterized by predictions having a coefficient of variation 0.1. A more comprehensive model that expresses $\text{COV } N / \text{COV } c_u$ as a function of $\delta_y / L.FS$ in addition to the $\text{COV } c_u$, the c_{u1}/c_{u2} ratio, and the slope angle β was established and proven to be more efficient at producing reliable predictions of $\text{COV } N / \text{COV } c_u$.

5. A practical design example that involved a two-layered slope system was used to show how the simple empirical models that were established in this thesis could be used to provide reliable estimates of the probability of failure of the slope system without the need for computationally demanding FLAC analyses with random fields. Estimates of the probability of failure could be obtained for different design factors of safety and for different conditions of slope geometry and soil properties.

APPENDIX I

FLAC CODE

```
new
call 01_Lib.dat
set cohesion_filename= 'V1.txt'
set cohesion_filename= 'J1.txt'
call 02_run.dat
call factorof.dat
-----
def variation
array proper(330)
status=open(cohesion_filename,0,1)
status=read(proper,330)
status=close
loop i(1,330)
proper(i)=parse(proper(i),1)
endloop
shadi=proper(1)
k=0
array bb(55,6)
    loop m(1,55)
        loop l(1,6)
            k=k+1
            bb(m,l)=proper(k)
        endloop
    endloop
reem=bb(7,2)
raj=bb(5,4)
command
    pri shadi
```

```

pri reem
    pri raj
endcommand
end

def function

    loop r(1,55)
        loop s(1,6)
            cohesion(r,s)=bb(r,s)
        endloop
    endloop
    ;cohesion(2,2)=bb(2,2)
    ;command
    ;pri cohesion
    ;endcommand
end

def variationn
array properr(595)
status=open(cohesion_filename,0,1)
status=read(properr,595)
status=close
loop ii(1,595)
properr(ii)=parse(properr(ii),1)
endloop
shadii=properr(1)
u=0
array bbb(35,17)
loop t(1,35)
loop v(1,17)
u=u+1

```

```

bbb(t,v)=properr(u)
endloop
endloop
reemm=bbb(9,5)
rajj=bbb(7,11)
command
pri shadii
pri reemm
pri rajj
endcommand
end
def functionn
f=0
loop rr(21,55)
dd=6
f=f+1
if f<36
loop ss(1,17)
dd=dd+1
if dd<24
cohesion(rr,dd)=bbb(f,ss)
endloop
endif
endif
endloop
command
pri cohesion
endcommand
end
; Source: Simple slope
;Units: SI: meter-kilogram-second

```

```

set gravity 9.81 ; m/s2
config
grid 55,23
gen 0.0,0.0 0.0,10.0 35.0,10.0 35.0,0.0 i=1,21 j=1,7
gen 35.0,0.0 35.0,10.0 104.64102,10.0 104.64102,0.0 i=21,56 j=1,7
gen 35.0,10.0 69.64102,30.0 104.64102,30.0 104.64102,10.0 i=21,56 j=7,24
; Define material models
group 'upper layer:new1' i=21,55 j=7,23
group 'lower layer:new2' i=1,20 j=1,6
group 'lower layer:new2' i=21,55 j=1,6
model mohr group 'upper layer:new1'
prop density=2039.5 bulk=1.333333E8 shear=1.37931E7 cohesion=100000.0 friction=0.0 dilation=0.0
tension=0.0 group 'upper layer:new1'
model mohr group 'lower layer:new2'
prop density=1835.5 bulk=1.333333E8 shear=1.37931E7 cohesion=20000.0 friction=0.0 dilation=0.0
tension=0.0 group 'lower layer:new2'
; Fixed boundary conditions
fix x i=1 j=1,7
fix x y i=1,21 j=1
fix x i=56 j=1,7
fix x y i=21,56 j=1
fix x i=56 j=7,24
set gravity=10.0 ; m/s2
variation
function
variationn
functionn

; This state should NOT be changed.
history 999 unbalanced
solve fos no_restore file=FoSmode1.fsv

```


save trial1.sav

def factor

array arrsave(1501)

array arra(1)

status=open('resultss.txt',0,1)

status=read(arr,1)

nlines=parse(arr(1),1)

if nlines>0

loop n(1,nlines)

status=read(arr,1)

arrsave(n)=arr(1)

endloop

endif

nlines=nlines+1

status=close

status=open('resultss.txt',1,1)

arra(1)=string(nlines)

status=write(arr,1)

if nlines>1

loop n(1,nlines-1)

arra(1)=arrsave(n)

status=write(arr,1)

endloop

endif

arra(1)=string(fos)

status=write(arr,1)

status=close

end

factor

```
def setup

array arra(1)
statuss=open('resultss.txt',1,1)
arra(1)=string(0)
statuss=write(arras,1)
statuss=close
end
setup
```

APPENDIX II

R SOFTWARE CODE

```
require(graphics)
require(mvtnorm)
require(truncdist)

iy=4      #Y-coordinate of the interface between layers

clx1=40   #Horizontal correlation length of layer 1 (top)
cly1=4    #Vertical correlation length of layer 1 (top)
clx2=40   #Horizontal correlation length of layer 2 (bottom)
cly2=4    #Vertical correlation length of layer 2 (bottom)

nr=1500   #Number of realizations/simulations

msu1=100  #Mean of undrained shear strength of layer 1
covsu1=0.4 #cov of undrained shear strength of layer 1

msu2=50   #Mean of undrained shear strength of layer 2
covsu2=0.4 #cov of undrained shear strength of layer 2

da=(read.csv("F:/FLACfile/PART Two/Uncertain Cases-Angle 45/Case 262/geometry1.csv"))
da=data.frame(N=seq(1,length(da[,1]),1),X=da[,1],Y=da[,2])
#plot(da$Y~da$X)
#plot(da[da$Y>10,]$Y~da[da$Y>10,]$X)

#####
```

```

#####
#Layer 1(top)
da1=da[da$Y>=iy,]

#constructing dx and dy matrices for layer 1
dx1=matrix(rep(NA,length(da1$X)^2),length(da1$X),length(da1$X))
dy1=matrix(rep(NA,length(da1$X)^2),length(da1$X),length(da1$X))
for (i in 1:length(da1$X)){
  for (j in 1:length(da1$X)){
    dx1[i,j]=abs(da1$X[i]-da1$X[j])
    dy1[i,j]=abs(da1$Y[i]-da1$Y[j])
  }
}
#Constructing Correlation matrix for layer 1
cormat1=exp(-(2*dx1/clx1+2*dy1/cly1))
isSymmetric(cormat1)

AB1 <- rmvnorm(mean=rep(0,length(da1$X)),sig=cormat1,n=nr) #Our gaussian variables
U1 <- pnorm(AB1) #Now U is uniform - check using hist(U[,1]) or hist(U[,2])
#ratio <- qtrunc(U[,1],spec="lnorm",a=1,b=Inf,2,.2) #x is gamma distributed

sdsulog=sqrt(log(1+covsu1^2))
msulog=log(msu1)-sdsulog^2/2

UU1=matrix(rep(NA,I(length(da1$X)*nr)),nr,length(da1$X))

for (i in 1:length(da1$X)){
  UU1[,i]=qtrunc(U1[,i],spec="lnorm",a=0,b=Inf,msulog,sdsulog)
}

```

```

UU1=UU1*1000
write.csv(t(UU1),"F:/FLACfile/PART Two/Uncertain Cases-Angle 45/Case 262/realization1.csv")

rmax=rep(NA,nr)
rmin=rep(NA,nr)
rmean=rep(NA,nr)
for (i in 1:nr){
  rmax[i]=max(UU1[i,])
  rmin[i]=min(UU1[i,])
  rmean[i]=mean(UU1[i,])
}
max(rmax)
min(rmin)
mean(rmean)

#####
#####
#####

#Layer 2(bottom)
da2=da[da$Y<iy,]

#constructing dx and dy matrices for layer 2
dx2=matrix(rep(NA,length(da2$X)^2),length(da2$X),length(da2$X))
dy2=matrix(rep(NA,length(da2$X)^2),length(da2$X),length(da2$X))
for (i in 1:length(da2$X)){
  for (j in 1:length(da2$X)){
    dx2[i,j]=abs(da2$X[i]-da2$X[j])
    dy2[i,j]=abs(da2$Y[i]-da2$Y[j])
  }
}

```

```

}
#Constructing Correlation matrix for layer 2
cormat2=exp(-(2*dx2/clx2+2*dy2/cly2))
isSymmetric(cormat2)

AB2 <- rmvnorm(mean=rep(0,length(da2$X)),sig=cormat2,n=nr) #Our gaussian variables
U2 <- pnorm(AB2) #Now U is uniform - check using hist(U[,1]) or hist(U[,2])
#ratio <- qtrunc(U[,1],spec="lnorm",a=1,b=Inf,2,.2) #x is gamma distributed

sdsulog=sqrt(log(1+covsu2^2))
msulog=log(msu2)-sdsulog^2/2

UU2=matrix(rep(NA,I(length(da2$X)*nr)),nr,length(da2$X))
for (i in 1:nr){
  UU2[i,]=qtrunc(U2[i,],spec="lnorm",a=0,b=Inf,msulog,sdsulog)
}
UU2=UU2*1000
write.csv(t(UU2),"F:/FLACfile/PART Two/Uncertain Cases-Angle 45/Case 262/realization2.csv")

rmax=rep(NA,nr)
rmin=rep(NA,nr)
rmean=rep(NA,nr)
for (i in 1:nr){
  rmax[i]=max(UU2[i,])
  rmin[i]=min(UU2[i,])
  rmean[i]=mean(UU2[i,])
}
max(rmax)
min(rmin)
mean(rmean)

```

APPENDIX III

VALIDATION CASES

Table 2. The values of the main factors in the N_m and COV N equations for the validation cases

$\delta_y/f.s$	$\delta_y /L.F.S$	c_{u1}/c_{u2}	β	d/H	COV c_u
0.20	0.07	5	30	2	0.4
0.67	0.10	1.5	45	1.5	0.4
0.13	0.04	4	30	3	0.5
0.10	0.04	2	60	2	0.3
0.27	0.09	5	45	3	0.5
0.40	0.16	3	60	1.5	0.3
0.10	0.03	1.5	30	4	0.5
0.25	0.08	3	30	4	0.3
0.20	0.07	5	40	2	0.5
0.50	0.18	1.5	50	2	0.5
0.20	0.06	4	40	4	0.2
0.30	0.11	4	50	2	0.4
0.20	0.09	2	50	3	0.4
0.30	0.11	4	45	2	0.2
0.50	0.18	5	40	2	0.3
0.13	0.05	2	30	1.5	0.4
0.27	0.09	4	60	3	0.5
0.15	0.05	4	30	4	0.4
0.13	0.05	4	50	3	0.3
0.07	0.02	5	60	3	0.4

BIBLIOGRAPHY

- Abusharar, S. W., & Han, J. (2011). Two-dimensional deep-seated slope stability analysis of embankments over stone column-improved soft clay. *Engineering Geology*, 120(1-4), 103-110.
- Babu, G. L. S., and Mukesh, M. D. (2004). Effect of soil variability on reliability of soil slopes. *Geotechnique*, 54(5), 335–337.
- Cho, S. E., (2007). Effects of spatial variability of soil properties on slope stability. *Eng. Geol.*, 92(3-4), 97-109.
- Cho, S.E., (2010). Probabilistic assessment of slope stability that considers the spatial variability of soil properties. *ASCE. Journal of Geotechnical and Geoenvironmental Engineering*, 136; 975–984.0.
- Griffiths, D. V., and Fenton, G. A., (2000). Influence of soil strength spatial variability on the stability of an undrained clay slope by finite elements. *Slope Stability*, 184-193.
- Griffiths, D. V., and Fenton, G. A. (2004). Probabilistic slope stability analysis by finite elements. *J. Geotech. Geoenviron. Eng.*, 130(5), 507-518.
- Griffiths, D.V., Huang, J., and Fenton, G. (2009). Influence of spatial variability on slope reliability using 2-D random fields. *J. Geotech. Geoenviron. Eng.* 135(10): 1367–1378.
- Griffiths, D. V., Huang, J., and Fenton, G., (2010). Comparison of slope reliability methods of analysis. *GeoFlorida*, 1952-1961.

- Griffiths, D. V. and Lane, P. A. (1999). Slope stability analysis by finite elements. *Géotechnique*, 49(3):387–403.
- Hong, H. P., and Roh, G., (2008). Reliability evaluation of earth slopes. *J. Geotech. Engrg.*134, 1700-1705.
- Jha, S. and Ching, J. (2013). Simplified reliability method for spatially variable undrained engineered slopes. *Soils and Foundations*, 53(5), 708-719.
- Jiang, S., & Huang, J. (2016). Efficient slope reliability analysis at low-probability levels in spatially variable soils. *Computers and Geotechnics*, 75, 18-27.
- Jiang, S., Huang, J., Yao, C., & Yang, J. (2017). Quantitative risk assessment of slope failure in 2-D spatially variable soils by limit equilibrium method. *Applied Mathematical Modelling*, 47, 710-725.
- Li, D., Jiang, S., Cao, Z., Zhou, W., Zhou, C., & Zhang, L. (2014). A multiple response-surface method for slope reliability analysis considering spatial variability of soil properties. *Engineering Geology*, 187, 60-72.
- Li, D., Xiao, T., Cao, Z., Phoon, K.K, & Zhou, C. (2015). Efficient and consistent reliability analysis of soil slope stability using both limit equilibrium analysis and finite element analysis. *Applied Mathematical Modelling*, 40(9-10), 5216-5229.
- Li, D., Zheng D., Cao Z.J., Tang X.S., Phoon K.K., (2016). Response surface methods for slope reliability analysis: Review and comparison. *Engineering Geology* 203: 3-14.
- Li, K. and Lumb, p. (1987). Probabilistic design of slopes. *Can. Geotech. J.*, 24, 520-531.

- Liu, L., Cheng, Y., Wang, X., Zhang, S., & Wu, Z. (2017). System reliability analysis and risk assessment of a layered slope in spatially variable soils considering stratigraphic boundary uncertainty. *Computers and Geotechnics*, 89, 213-225.
- Low, B. K. (2003). Practical probabilistic slope stability analysis. Proc., Soil and Rock America 2003, 12th Panamerican Conf. on Soil Mechanics and Geotechnical Engineering, and 39th U.S. Rock Mechanics Symp., MIT, Cambridge, Mass., Vol. 2, Verlag Gluckauf GmbH, Essen, Germany, 2777-2784.
- Malkawi, A. I., Hassan, W. F., and Abdulla, F. A., (2000). Uncertainty and reliability analysis applied to slope stability. *Structural Safety* 22, 161-187.
- Qian, Z. G., A. J. Li, R. S. Merifield, and A. V. Lyamin, (2015). Slope Stability Charts for Two-Layered Purely Cohesive Soils Based on Finite-Element Limit Analysis Methods. *International Journal of Geomechanics* 15, no. 3: 06014022.
- Srivastava, A. (2012). Spatial Variability Modelling of Geotechnical Parameters and Stability of Highly Weathered Rock Slope. *Indian Geotechnical Journal*, 42(3), 179-185.
- Terzaghi, K. & Peck, R.B. (1948). *Soil Mechanics in Engineering Practice*, 1st Edition, John Wiley and Sons, New York.
- Vanmarcke, E. H. 1977. "Reliability of earth slopes." *J. Geotech. Engrg. Div.*, 10311, 1247-1265.

Wang, Y., Cao, Z., Au, S.-K., 2011. Practical reliability analysis of slope stability by advanced Monte Carlo simulations in a spreadsheet. *Canadian Geotechnical Journal* 48 (1), 162–172.

Zaskórski, Ł, Puła, W., & Griffiths, D. V. (2017). Bearing Capacity Assessment of a Shallow Foundation on a Two-Layered Soil Using the Random Finite Element Method. *Geo-Risk 2017*.

Zhu, D., Griffiths, D. V., Huang, J., & Fenton, G. A. (2017). Probabilistic stability analyses of undrained slopes with linearly increasing mean strength. *Géotechnique*, 1-14.